

Direct implementation of high order BGT artificial boundary conditions [☆]



M. Medvinsky ^a, S. Tsynkov ^{a,*}, E. Turkel ^b

^a Department of Mathematics, North Carolina State University, Box 8205, Raleigh, NC 27695, USA

^b School of Mathematical Sciences, Tel Aviv University, Ramat Aviv, Tel Aviv 69978, Israel

ARTICLE INFO

Article history:

Received 3 May 2018

Received in revised form 18 September 2018

Accepted 18 September 2018

Available online xxxx

Keywords:

Propagation of waves over unbounded regions

Helmholtz equation

Spherical artificial boundary

Expansion with respect to continuous basis

Method of difference potentials (MDP)

Beltrami operator

ABSTRACT

Local artificial boundary conditions (ABCs) for the numerical simulation of waves have been successfully used for decades (most notably, the boundary conditions due to Engquist & Majda, Bayliss, Gunzburger & Turkel, and Higdon). The basic idea behind these boundary conditions is that they cancel several leading terms in an expansion of the solution. The larger the number of terms canceled, the higher the order of the boundary condition and, in turn, the smaller the reflection error due to truncation of the original unbounded domain by an artificial outer boundary. In practice, however, the use of local ABCs has been limited to low orders (first and second), because higher order boundary conditions involve higher order derivatives of the solution, which may harm well-posedness and cause numerical instabilities. They are also difficult to implement especially in finite elements. A prominent exception is the development of local high order ABCs based on auxiliary variables.

In the current paper, we implement high order Bayliss–Turkel ABCs directly – with no auxiliary variables yet no discrete approximation of the constituent high order derivatives either. Instead, we represent the solution at the boundary as an expansion with respect to a continuous basis. For the spherical artificial boundary, the basis consists of eigenfunctions of the Beltrami operator (spherical harmonics), which enable replacing the high order derivatives in the ABCs with powers of the corresponding eigenvalues. The continuous representation at the boundary is coupled to higher order compact finite differences inside the domain by the method of difference potentials (MDP). It maintains high order accuracy even when the boundary is not aligned with the discretization grid.

© 2018 Elsevier Inc. All rights reserved.

1. Introduction

Describing the behavior of scattered waves about a body is essential in many fields, whether it be the reflection of sonar waves from a submarine, the reflection of radar waves from an airplane or the reflection of microwaves from a

[☆] Work supported by the US Army Research Office (ARO) under grant # W911NF-16-1-0115, and by the US-Israel Binational Science Foundation (BSF) under grant # 2014048.

* Corresponding author.

E-mail addresses: mmedvin@ncsu.edu (M. Medvinsky), tsynkov@math.ncsu.edu (S. Tsynkov), turkel@post.tau.ac.il (E. Turkel).

URLs: <https://mmedvin.math.ncsu.edu> (M. Medvinsky), <https://tsynkov.math.ncsu.edu> (S. Tsynkov), <http://www.math.tau.ac.il/~turkel/> (E. Turkel).

cellular phone. In computing such solutions, one, in principle, needs to compute on an unbounded domain. Analytically, the Sommerfeld condition allows only outgoing waves and eliminates those coming in from infinity.

Unfortunately, due the finiteness of the computer it is not feasible to compute on an unbounded domain. There are several approaches to overcoming this difficulty. The approach we use develops a finite difference (or finite element) approximation, which is grid based. One then adds an artificial outer surface. On this surface, an artificial boundary condition (ABC) is imposed that reduces the reflection of waves back into the domain of interest. Another approach would be to reformulate the partial differential equation as a boundary integral equation. This integral equation contains a Green's function which automatically allows only the correct behavior at infinity. Yet another approach would be to use finite elements that are unbounded (the so-called infinite elements [1]).

There are three main methods for the treatment of artificial outer boundaries for wave-like equations. Early techniques used local approximations. In particular, the approach by Engquist and Majda [2] relies on splitting the time-dependent equation into forward and backward parts and using pseudo-differential analysis to gain approximate ABCs. The approach by Higdon [3,4] makes the artificial boundary transparent for plane waves traveling at predetermined incidence angles. The approach by Bayliss and Turkel [5,6] is based on expansions in an inverse radius for both the time-dependent and time-harmonic cases. To improve the accuracy of local techniques, one can use non-local operators that may employ an integral or pseudo-differential formulation along the boundary. This is frequently expressed as a Dirichlet to Neumann map (DtN) [7–9]. An alternative to both local and non-local ABCs is provided by the approach initiated by Bérenger [10]. It constructs an exterior layer to the domain that matches the interior in a way to greatly reduce the reflections. This is usually referred to as a perfectly matched layer (PML).

In this work, we concentrate on the Bayliss–Gunzburger–Turkel (BGT) approach [6] for the 3D Helmholtz equation. The BGT algorithm constructs a sequence of increasingly more accurate ABCs; the accuracy increases as the spherical radius r increases, the wavenumber k increases, and the order of the ABC increases. In practice, however, only the first two BGT operators are used since higher order operators require high order tangential derivatives. This is especially difficult for finite element methods but is also a difficulty for finite difference methods. A similar difficulty affects the Engquist–Majda and Higdon sequences of operators. One way to overcome this difficulty is to add auxiliary variables instead of employing a larger stencil. This approach has been applied to the Engquist–Majda, Higdon, and BGT sequences of ABCs [11–17]. The Engquist–Majda and Higdon ABCs are most straightforward to use in Cartesian coordinates, while the BGT ABCs are easier to implement in polar or spherical coordinates. Zarmi and Turkel [18] consider a more general way of extending the BGT approach to other coordinate systems.

For wave-like equations it is well known that both finite differences and finite elements suffer from a pollution effect. This implies that the numerical error grows faster than linear with the frequency of the wave. This growth decreases as the rate of accuracy of the scheme increases. Hence, it is important to solve wave propagation problems with high order schemes. In practice, a fourth order or possibly sixth order accurate scheme is sufficient. In this paper, we solve the frequency domain wave equation, i.e., the Helmholtz equation, in three space dimensions using a sixth order accurate compact finite difference scheme [19].

The total error is therefore composed of two separate entities: the discretization error of the scheme in the interior of the domain and the error caused by reflections from the artificial outer boundary. In general, the global error will be dominated by the larger of these errors. Hence, it is important to reduce both sets of errors. As stated above, we will use a sixth order accurate compact finite difference scheme for the Helmholtz equation. In addition, we need to reduce the error from the BGT boundary condition, i.e., increase its order. In doing so, we would like to avoid using large stencils for the approximation of high order derivatives, as this is not practical.

Therefore, in this paper we introduce a new method of imposing high order BGT boundary conditions. It consists of first developing a sequence of explicit formulae for the ABC operators that involve powers of the Beltrami operator on the spherical artificial boundary. Then, the solution at the boundary is expanded in the basis of spherical harmonics that are eigenfunctions of the Beltrami operator. This reduces powers of the Beltrami operator in the ABCs to powers of the corresponding eigenvalues, and hence requires neither the approximation of high order tangential derivatives on large stencils nor the introduction of auxiliary variables. Finally, the BGT condition represented in the basis of spherical harmonics at the boundary is coupled with a sixth order finite difference scheme that approximates the Helmholtz equation on the domain via the method of difference potentials (MDP) [20]. The MDP enables high order accuracy even for non-conforming boundaries. In our case, the artificial boundary is spherical and the discretization grid is Cartesian.

Computational experiments are then performed to show the power of the new approach. As expected, both the wavenumber and the position of the artificial outer surface (i.e., the radius of the spherical domain) affect the accuracy of the ABC and thus the balance between the discretization and reflection error. As the outer surface is brought closer in (reducing the computational effort) or the wavenumber is reduced, there is a greater need for a high order ABC.

2. BGT boundary conditions

We derive convenient explicit formulae for the three dimensional BGT artificial boundary conditions. The high order tangential derivatives in the ABCs appear as powers of the spherical Beltrami operator. These formulae are of use by them-

selves. In addition, once applied on a sphere, they naturally facilitate an expansion in the basis of Beltrami eigenfunctions (spherical harmonics) so that high order derivatives transform into algebraic expressions – powers of the eigenvalues.

The Helmholtz equation in spherical coordinates is given by

$$\frac{\partial^2 u}{\partial r^2} + \frac{2}{r} \frac{\partial u}{\partial r} + \frac{\Delta_{\theta,\varphi} u}{r^2} + k^2 u = 0, \tag{1}$$

where $\Delta_{\theta,\varphi}$ is the Laplacian with respect to spherical angles θ and φ , i.e. the Beltrami operator:

$$\Delta_{\theta,\varphi} u = \frac{1}{\sin \theta} \frac{\partial}{\partial \theta} \left(\sin \theta \frac{\partial u}{\partial \theta} \right) + \frac{1}{\sin^2 \theta} \frac{\partial^2 u}{\partial \varphi^2}. \tag{2}$$

A Bayliss–Gunzburger–Turkel (BGT) ABC [6] of order m is given by the operator relation $B_m u = 0$, where $B_0 = I$ and the subsequent operators B_m are defined recursively:

$$B_m u = \left(\frac{\partial}{\partial r} - ik + \frac{2m-1}{r} \right) B_{m-1} u, \quad m = 1, 2, 3, \dots \tag{3}$$

The first three boundary operators B_m from sequence (3) are:

$$\begin{aligned} B_1 u &= \frac{\partial u}{\partial r} - ik u + \frac{u}{r}, \\ B_2 u &= \frac{\partial^2 u}{\partial r^2} + 2 \left(\frac{2}{r} - ik \right) \frac{\partial u}{\partial r} + \left(\frac{2}{r^2} - \frac{4ik}{r} - 2k^2 \right) u \\ &= 2 \left(\frac{1}{r} - ik \right) \frac{\partial u}{\partial r} - \frac{\Delta_{\theta,\varphi} u}{r^2} + \left(\frac{-4ik}{r} + \frac{2}{r^2} - 2k^2 \right) u, \\ B_3 u &= \left(-\frac{12ik}{r} - 4k^2 + \frac{6}{r^2} \right) \frac{\partial u}{\partial r} - \frac{1}{r^2} \Delta_{\theta,\varphi} \frac{\partial u}{\partial r} \\ &\quad + \left(-\frac{5}{r^3} + \frac{3ik}{r^2} \right) \Delta_{\theta,\varphi} u + \left(4ik^3 - \frac{16k^2}{r} - \frac{18ik}{r^2} + \frac{6}{r^3} \right) u. \end{aligned} \tag{4}$$

Explicit expressions for higher order operators up to $m = 6$ are given in Section 2.3. Using the Helmholtz equation, all operators B_m can be reduced to a first derivative with respect to r and tangential derivatives. In particular, $B_4 u$ contains u , $\frac{\partial u}{\partial r}$, $\Delta_{\theta,\varphi} u$, $\Delta_{\theta,\varphi}^2 u$, and $\Delta_{\theta,\varphi} \frac{\partial u}{\partial r}$.

As shown in [6], the BGT boundary condition of order m , $B_m u = 0$, cancels out the m leading terms in the following far-field expansion of the solution u to equation (1):

$$u(r, \theta, \varphi) = \frac{e^{ikr}}{kr} \sum_{j=0}^{\infty} \frac{F_j(\theta, \varphi)}{(kr)^j}. \tag{5}$$

In formula (5), $F_0(\theta, \varphi)$ is known as the far-field radiation pattern, and all subsequent $F_j(\theta, \varphi)$ for $j > 0$ can be obtained from $F_0(\theta, \varphi)$ by means of explicit recursive relations. The rationale behind designing the ABCs this way is obvious. If m leading terms are cancelled, the reflection error is controlled by the largest remaining term in expansion (5), which is proportional to $(kr)^{-m-1}$. Therefore, for a BGT ABC set at the outer boundary $r = R$, the reflection error is expected to decrease as the order m increases (as long as $kR > 1$). The reflection error is also expected to decrease for larger R and for larger k (i.e., shorter waves). In Section 5, we corroborate these expectations with numerical results.

2.1. Derivation of the explicit BGT formulae

In this section, we use a simplified notation Δ instead of $\Delta_{\theta,\varphi}$. The following theorem yields the expressions for the operators B_m . The cases of even and odd m are considered separately.

Theorem 1. Case 1, m is even (and $m - 1$ is odd):

$$\begin{aligned} B_{m-1} u &= \alpha_{m-1} \frac{\partial u}{\partial r} + \sum_{n=1}^{\frac{m}{2}-1} \beta_{m-1,n} \Delta^n u + \sum_{n=1}^{\frac{m}{2}-1} \gamma_{m-1,n} \Delta^n \frac{\partial u}{\partial r} + \delta_{m-1} u, \\ B_m u &= \alpha_m \frac{\partial u}{\partial r} + \sum_{n=1}^{\frac{m}{2}} \beta_{m,n} \Delta^n u + \sum_{n=1}^{\frac{m}{2}-1} \gamma_{m,n} \Delta^n \frac{\partial u}{\partial r} + \delta_m u. \end{aligned} \tag{6}$$

Case 2, m is odd (and $m - 1$ is even):

$$\begin{aligned}
 B_{m-1}u &= \alpha_{m-1} \frac{\partial u}{\partial r} + \sum_{n=1}^{\frac{m-1}{2}} \beta_{m-1,n} \Delta^n u + \sum_{n=1}^{\frac{m-3}{2}} \gamma_{m-1,n} \Delta^n \frac{\partial u}{\partial r} + \delta_{m-1}u, \\
 B_m u &= \alpha_m \frac{\partial u}{\partial r} + \sum_{n=1}^{\frac{m-1}{2}} \beta_{m,n} \Delta^n u + \sum_{n=1}^{\frac{m-1}{2}} \gamma_{m,n} \Delta^n \frac{\partial u}{\partial r} + \delta_{m-1}u.
 \end{aligned}
 \tag{7}$$

In formulae (6)–(7), α , β , γ , and δ are functions of r only.

The difference between the two cases in Theorem 1 is the upper limit in the sums. One can see that when m is even we add an extra term $\Delta^n u$ and when m is odd we add a new term $\Delta^n \frac{\partial u}{\partial r}$.

Proof. We prove Theorem 1 by induction. It holds for $m = 1$ by inspection. Next, we assume that it is true for a given B_{m-1} and show that then the expression for B_m also holds. We first treat both cases, (6) and (7), together and do not display the upper limits in the various sums.

Using equation (3), we can write:

$$\begin{aligned}
 B_m u &= \alpha_{m-1} \frac{\partial^2 u}{\partial r^2} + \alpha'_{m-1} \frac{\partial u}{\partial r} + \sum_n \beta'_{m-1,n} \Delta^n u + \sum_n \beta_{m-1,n} \Delta^n \frac{\partial u}{\partial r} \\
 &+ \sum_n \gamma'_{m-1,n} \Delta^n \frac{\partial u}{\partial r} + \sum_n \gamma_{m-1,n} \Delta^n \frac{\partial^2 u}{\partial r^2} + \delta'_{m-1}u + \delta_{m-1} \frac{\partial u}{\partial r} \\
 &+ \left(-ik + \frac{2m-1}{r}\right) \left[\alpha_{m-1} \frac{\partial u}{\partial r} + \sum_n \beta_{m-1,n} \Delta^n u + \sum_n \gamma_{m-1,n} \Delta^n \frac{\partial u}{\partial r} + \delta_{m-1}u\right] \\
 &= \left[\alpha_{m-1} + \sum_n \gamma_{m-1,n} \Delta^n\right] \frac{\partial^2 u}{\partial r^2} + \left[\alpha'_{m-1} + \delta_{m-1} + \left(-ik + \frac{2m-1}{r}\right)\alpha_{m-1}\right] \frac{\partial u}{\partial r} \\
 &+ \left[\sum_n (\beta_{m-1,n} + \gamma'_{m-1,n}) + \left(-ik + \frac{2m-1}{r}\right)\gamma_{m-1,n}\right] \Delta^n \frac{\partial u}{\partial r} \\
 &+ \left[\delta'_{m-1} + \left(-ik + \frac{2m-1}{r}\right)\delta_{m-1}\right]u \\
 &+ \left[\sum_n \beta'_{m-1,n} + \left(-ik + \frac{2m-1}{r}\right)\sum_n \beta_{m-1,n}\right] \Delta^n u,
 \end{aligned}$$

where primes denote differentiation with respect to r , e.g., $\alpha'_{m-1} = \frac{d\alpha_{m-1}}{dr}$. The second derivative $\frac{\partial^2 u}{\partial r^2}$ can be eliminated with the help of the Helmholtz equation (1). Therefore:

$$\begin{aligned}
 B_m u &= \left[\alpha'_{m-1} + \delta_{m-1} - \frac{2\alpha_{m-1}}{r} + \left(-ik + \frac{2m-1}{r}\right)\alpha_{m-1}\right] \frac{\partial u}{\partial r} \\
 &+ \left[\sum_n (\beta_{m-1,n} + \gamma'_{m-1,n}) + \left(-ik + \frac{2m-3}{r}\right)\gamma_{m-1,n}\right] \Delta^n \frac{\partial u}{\partial r} \\
 &+ \left[\delta'_{m-1} - \alpha_{m-1}k^2 + \left(-ik + \frac{2m-1}{r}\right)\delta_{m-1}\right]u \\
 &+ \left[\sum_n (\beta'_{m-1,n} - k^2\gamma_{m-1,n}) + \left(-ik + \frac{2m-1}{r}\right)\sum_n \beta_{m-1,n}\right] \Delta^n u \\
 &- \frac{\alpha_{m-1}\Delta u}{r^2} - \frac{1}{r^2} \sum_n \gamma_{m-1,n} \Delta^{n+1}u.
 \end{aligned}$$

Next, we re-insert the upper limits separately for the cases of even and odd m .

Case 1, m is even:

$$\begin{aligned}
 B_m u &= \left[\alpha'_{m-1} + \delta_{m-1} - \frac{2\alpha_{m-1}}{r} + \left(-ik + \frac{2m-1}{r}\right) \alpha_{m-1} \right] \frac{\partial u}{\partial r} \\
 &+ \left[\sum_{n=1}^{\frac{m}{2}-1} (\beta_{m-1,n} + \gamma'_{m-1,n}) + \left(-ik + \frac{2m-3}{r}\right) \gamma_{m-1,n} \right] \Delta^n \frac{\partial u}{\partial r} \\
 &+ \left[\delta'_{m-1} - \alpha_{m-1} k^2 + \left(-ik + \frac{2m-1}{r}\right) \delta_{m-1} \right] u \\
 &+ \left[\sum_{n=1}^{\frac{m}{2}-1} (\beta'_{m-1,n} - k^2 \gamma_{m-1,n}) + \left(-ik + \frac{2m-1}{r}\right) \sum_{n=1}^{\frac{m}{2}-1} \beta_{m-1,n} \right] \Delta^n u \\
 &- \frac{\alpha_{m-1} \Delta u}{r^2} - \frac{1}{r^2} \sum_{n=1}^{\frac{m}{2}-1} \gamma_{m-1,n} \Delta^{n+1} u.
 \end{aligned} \tag{8}$$

Case 2, m is odd:

$$\begin{aligned}
 B_m u &= \left[\alpha'_{m-1} + \delta_{m-1} - \frac{2\alpha_{m-1}}{r} + \left(-ik + \frac{2m-1}{r}\right) \alpha_{m-1} \right] \frac{\partial u}{\partial r} \\
 &+ \left[\sum_{n=1}^{\frac{m-1}{2}} \beta_{m-1,n} + \sum_{n=1}^{\frac{m-3}{2}} \gamma'_{m-1,n} + \left(-ik + \frac{2m-3}{r}\right) \sum_{n=1}^{\frac{m-3}{2}} \gamma_{m-1,n} \right] \Delta^n \frac{\partial u}{\partial r} \\
 &+ \left[\delta'_{m-1} - \alpha_{m-1} k^2 + \left(-ik + \frac{2m-1}{r}\right) \delta_{m-1} \right] u \\
 &+ \left[\sum_{n=1}^{\frac{m-1}{2}} \beta'_{m-1,n} - k^2 \sum_{n=1}^{\frac{m-3}{2}} \gamma_{m-1,n} + \left(-ik + \frac{2m-1}{r}\right) \sum_{n=1}^{\frac{m-1}{2}} \beta_{m-1,n} \right] \Delta^n u \\
 &- \frac{\alpha_{m-1} \Delta u}{r^2} - \frac{1}{r^2} \sum_{n=1}^{\frac{m-3}{2}} \gamma_{m-1,n} \Delta^{n+1} u.
 \end{aligned} \tag{9}$$

Comparing (6) with (8) and (7) with (9), we have the following recursive relations for the coefficients:

$$\begin{aligned}
 \alpha_m &= \alpha'_{m-1} + \left(\frac{2m-3}{r} - ik \right) \alpha_{m-1} + \delta_{m-1}, \\
 \beta_{m,1} &= \beta'_{m-1,1} + \left(\frac{2m-1}{r} - ik \right) \beta_{m-1,1} - \gamma_{m-1,1} k^2 - \frac{\alpha_{m-1}}{r^2}, \\
 \beta_{m,n} &= \beta'_{m-1,n} + \left(\frac{2m-1}{r} - ik \right) \beta_{m-1,n} - \gamma_{m-1,n} k^2 - \frac{\gamma_{m-1,n-1}}{r^2}, \quad n > 1, \\
 \gamma_{m,n} &= \gamma'_{m-1,n} + \left(\frac{2m-3}{r} - ik \right) \gamma_{m-1,n} + \beta_{m-1,n}, \\
 \delta_m &= \delta'_{m-1} + \left(\frac{2m-1}{r} - ik \right) \delta_{m-1} - \alpha_{m-1} k^2,
 \end{aligned} \tag{10}$$

subject to the initial conditions at $m = 1$:

$$\begin{aligned}
 \alpha_1 &= 1, \\
 \beta_{1,n} &= 0, \quad \forall n, \\
 \gamma_{1,n} &= 0, \quad \forall n, \\
 \delta_1 &= \frac{1}{r} - ik.
 \end{aligned} \tag{11}$$

Primes on the right-hand sides of equations (10) denote differentiation with respect to r . \square

2.2. Coefficients

Lemma 2. δ_m depends on α_m as follows:

$$\delta_m = \left(\frac{1}{r} - ik\right) \alpha_m, \quad \forall m.$$

Proof. By induction:

1. Lemma 2 holds for δ_1 due to the initial conditions (11).
2. Assuming that $\delta_{m-1} = (\frac{1}{r} - ik)\alpha_{m-1}$, we derive δ_m using (10):

$$\begin{aligned} \delta_m &= \delta'_{m-1} + \left(\frac{2m-1}{r} - ik\right) \delta_{m-1} - \alpha_{m-1}k^2 \\ &= \left(\left(\frac{1}{r} - ik\right) \alpha_{m-1}\right)' + \left(\frac{2m-1}{r} - ik\right) \left(\frac{1}{r} - ik\right) \alpha_{m-1} - \alpha_{m-1}k^2 \\ &= \left(\frac{1}{r} - ik\right) \alpha'_{m-1} - \frac{1}{r^2} \alpha_{m-1} + \left(\frac{2m-1}{r} - ik\right) \left(\frac{1}{r} - ik\right) \alpha_{m-1} - \alpha_{m-1}k^2 \\ &= \left(\frac{1}{r} - ik\right) \left(\alpha'_{m-1} + \left(\frac{2m-1}{r} - ik\right) \alpha_{m-1}\right) - \left(\frac{1}{r} - ik\right) \left(\frac{1}{r} + ik\right) \alpha_{m-1} \\ &= \alpha'_{m-1} + 2\left(\frac{m-1}{r} - ik\right) \alpha_{m-1} \\ &= \left(\frac{1}{r} - ik\right) \alpha_m. \end{aligned}$$

The last equality holds since

$$\begin{aligned} \alpha_m &= \alpha'_{m-1} + \left(\frac{2m-3}{r} - ik\right) \alpha_{m-1} + \delta_{m-1} \\ &= \alpha'_{m-1} + \left(\frac{2m-3}{r} - ik\right) \alpha_{m-1} + \left(\frac{1}{r} - ik\right) \alpha_{m-1} \\ &= \alpha'_{m-1} + 2\left(\frac{m-1}{r} - ik\right) \alpha_{m-1}. \quad \square \end{aligned}$$

Lemma 3 (Vanishing condition for $\beta_{m,n}$ and $\gamma_{m,n}$).

$$\begin{cases} \beta_{m,n} = 0, & n > \lfloor \frac{m}{2} \rfloor, \\ \gamma_{m,n'} = 0, & n' > \lfloor \frac{m-1}{2} \rfloor, \end{cases}$$

where the floor function $\lfloor \cdot \rfloor$ is the largest integer that does not exceed the argument.

Proof. By induction on m :

1. Lemma 3 holds for $\beta_{1,n}$ and $\gamma_{1,n'}$ due to the initial conditions (11).
2. Assume that

$$\begin{cases} \beta_{m-1,\tilde{n}} = 0, & \tilde{n} > \lfloor \frac{m-1}{2} \rfloor, \\ \gamma_{m-1,\tilde{n}'} = 0, & \tilde{n}' > \lfloor \frac{m-2}{2} \rfloor. \end{cases}$$

Note that the assumption implies that $\beta'_{m-1,\tilde{n}} = 0$ and $\gamma'_{m-1,\tilde{n}'} = 0$.

Using (10) for $n > \lfloor \frac{m}{2} \rfloor \geq \lfloor \frac{m-1}{2} \rfloor$ and $n' > \lfloor \frac{m-1}{2} \rfloor \geq \lfloor \frac{m-2}{2} \rfloor$ one gets

$$\begin{aligned} \beta_{m,n} &= \beta'_{m-1,n} + \left(\frac{2m-1}{r} - ik\right) \beta_{m-1,n} - \gamma_{m-1,n}k^2 - \frac{\gamma_{m-1,n-1}}{r^2} = -\frac{\gamma_{m-1,n-1}}{r^2}, \\ \gamma_{m,n'} &= \gamma'_{m-1,n'} + \left(\frac{2m-3}{r} - ik\right) \gamma_{m-1,n'} + \beta_{m-1,n'} = \beta_{m-1,n'} = 0. \end{aligned}$$

Note that $n-1 > \lfloor \frac{m}{2} \rfloor - 1 = \lfloor \frac{m-2}{2} \rfloor$, so $\gamma_{m-1,n-1} = 0$ and the proof is completed. \square

Corollary 4. The following simplified formula yields the operators B_m :

$$B_m u = \alpha_m \frac{\partial u}{\partial r} + \sum_{n=1}^{\lfloor \frac{m}{2} \rfloor} \beta_{m,n} \Delta_{\theta,\varphi}^n u + \sum_{n=1}^{\lfloor \frac{m-1}{2} \rfloor} \gamma_{m,n} \Delta_{\theta,\varphi}^n \frac{\partial u}{\partial r} + \left(\frac{1}{r} - ik \right) \alpha_m u, \quad (12)$$

where the coefficients are defined recursively:

$$\begin{aligned} \alpha_m &= \alpha'_{m-1} + 2 \left(\frac{m-1}{r} - ik \right) \alpha_{m-1}, \\ \beta_{m,1} &= \beta'_{m-1,1} + \left(\frac{2m-1}{r} - ik \right) \beta_{m-1,1} - \gamma_{m-1,1} k^2 - \frac{\alpha_{m-1}}{r^2}, \\ \beta_{m,n} &= \beta'_{m-1,n} + \left(\frac{2m-1}{r} - ik \right) \beta_{m-1,n} - \gamma_{m-1,n} k^2 - \frac{\gamma_{m-1,n-1}}{r^2}, \quad n > 1, \\ \gamma_{m,n} &= \gamma'_{m-1,n} + \left(\frac{2m-3}{r} - ik \right) \gamma_{m-1,n} + \beta_{m-1,n}, \end{aligned}$$

subject to the initial conditions at $m = 1$:

$$\begin{aligned} \alpha_1 &= 1, \\ \beta_{1,n} &= 0, \quad \forall n, \\ \gamma_{1,n} &= 0, \quad \forall n. \end{aligned}$$

2.3. High-order BGT operators

The operators B_m for $m = 1, 2$, and 3 are given by equation (4). Here, we display B_m explicitly for $m = 4, 5$, and 6 :

$$\begin{aligned} B_4 u &= \frac{1}{r^4} \Delta_{\theta,\varphi}^2 u + \left(\frac{8k^2}{r^2} + \frac{32ik}{r^3} - \frac{26}{r^4} \right) \Delta_{\theta,\varphi} u + \left(8k^4 + \frac{56ik^3}{r} - \frac{120k^2}{r^2} - \frac{96ik}{r^3} + \frac{24}{r^4} \right) u \\ &\quad + \left(-\frac{8}{r^3} + \frac{4ik}{r^2} \right) \Delta_{\theta,\varphi} \frac{\partial u}{\partial r} + \left(8ik^3 - \frac{48k^2}{r} - \frac{72ik}{r^2} + \frac{24}{r^3} \right) \frac{\partial u}{\partial r}, \\ B_5 u &= \frac{1}{r^4} \Delta_{\theta,\varphi}^2 \frac{\partial u}{\partial r} + \left(\frac{12k^2}{r^2} + \frac{60ik}{r^3} - \frac{58}{r^4} \right) \Delta_{\theta,\varphi} \frac{\partial u}{\partial r} \\ &\quad + \left(16k^4 + \frac{160ik^3}{r} - \frac{480k^2}{r^2} - \frac{480ik}{r^3} + \frac{120}{r^4} \right) \frac{\partial u}{\partial r} \\ &\quad + \left(\frac{13}{r^5} - \frac{5ik}{r^4} \right) \Delta_{\theta,\varphi}^2 u + \left(-\frac{20ik^3}{r^2} + \frac{144k^2}{r^3} + \frac{290ik}{r^4} - \frac{154}{r^5} \right) \Delta_{\theta,\varphi} u \\ &\quad + \left(-16ik^5 + \frac{176k^4}{r} + \frac{640ik^3}{r^2} - \frac{960k^2}{r^3} - \frac{600ik}{r^4} + \frac{120}{r^5} \right) u, \\ B_6 u &= \left(\frac{18}{r^5} - \frac{6ik}{r^4} \right) \Delta_{\theta,\varphi}^2 \frac{\partial u}{\partial r} + \left(-\frac{32ik^3}{r^2} + \frac{288k^2}{r^3} + \frac{708ik}{r^4} - \frac{444}{r^5} \right) \Delta_{\theta,\varphi} \frac{\partial u}{\partial r} \\ &\quad + \left(-32ik^5 + \frac{480k^4}{r} + \frac{2400ik^3}{r^2} - \frac{4800k^2}{r^3} - \frac{3600ik}{r^4} + \frac{720}{r^5} \right) \frac{\partial u}{\partial r} - \frac{1}{r^6} \Delta_{\theta,\varphi}^3 u \\ &\quad + \left(-\frac{18k^2}{r^4} - \frac{108ik}{r^5} + \frac{136}{r^6} \right) \Delta_{\theta,\varphi}^2 u \\ &\quad + \left(-\frac{48k^4}{r^2} - \frac{544ik^3}{r^3} + \frac{1980k^2}{r^4} + \frac{2664ik}{r^5} - \frac{1044}{r^6} \right) \Delta_{\theta,\varphi} u \\ &\quad + \left(-32k^6 - \frac{512ik^5}{r} + \frac{2880k^4}{r^2} + \frac{7200ik^3}{r^3} - \frac{8400k^2}{r^4} - \frac{4320ik}{r^5} + \frac{720}{r^6} \right) u. \end{aligned} \quad (13)$$

Formulae (13) along with formulae (4) yield explicit representation of the BGT ABCs $B_m u = 0$, $m = 1, \dots, 6$, in terms of original variables.

3. Spherical harmonics

Let $Y_l^s = Y_l^s(\theta, \varphi)$ denote spherical harmonics:

$$Y_l^s(\theta, \varphi) = \mathcal{P}_l^{|s|}(\cos \theta)e^{is\varphi}, \quad 0 \leq \theta \leq \pi, \quad 0 \leq \varphi < 2\pi, \tag{14}$$

$$l = 0, 1, 2, \dots, \quad s = -l, \dots, 0, \dots, l,$$

where $\mathcal{P}_l^s = \mathcal{P}_l^s(x)$ are the associated Legendre functions:

$$\mathcal{P}_l^s(x) = (1-x^2)^{\frac{s}{2}} \frac{d^s}{dx^s} \mathcal{P}_l(x), \quad l = 0, 1, 2, \dots, \quad s = 0, 1, 2, \dots, l, \tag{15}$$

and $\mathcal{P}_l = \mathcal{P}_l(x)$ are the Legendre polynomials:

$$\mathcal{P}_l(x) = \frac{1}{2^l l!} \frac{d^l}{dx^l} (x^2 - 1)^l, \quad l = 0, 1, 2, \dots$$

It is well known that the spherical harmonics (14) are eigenfunctions of the Beltrami operator $\Delta_{\theta, \varphi}$ of (2):

$$\Delta_{\theta, \varphi} Y_l^s = -l(l+1)Y_l^s, \quad l = 0, 1, 2, \dots, \quad s = -l, \dots, 0, \dots, l, \tag{16}$$

where the eigenvalue $\lambda = -l(l+1)$ has multiplicity $2l+1$. Moreover, the spherical harmonics $Y_l^s = Y_l^s(\theta, \varphi)$ of (14) form a complete orthogonal system in the space L_2 on the unit sphere.

Let $u = u(r, \theta, \varphi)$ be a solution to the Helmholtz equation (1) that satisfies the BGT boundary condition $B_m u = 0$ at the spherical artificial boundary $r = R = \text{const}$. The operator B_m is defined by formula (12). Both u and $\frac{\partial u}{\partial r}$ at a fixed $r = R$ are functions of the spherical angles θ and φ only. Hence, both can be expanded with respect to the spherical harmonics:

$$u(R, \theta, \varphi) = \sum_{l,s} c_{ls}^{(0)} Y_l^s(\theta, \varphi), \tag{17a}$$

$$\frac{\partial u}{\partial r}(R, \theta, \varphi) = \sum_{l,s} c_{ls}^{(1)} Y_l^s(\theta, \varphi), \tag{17b}$$

where the coefficients $c_{ls}^{(0)}$ of (17a) and $c_{ls}^{(1)}$ of (17b) are given by:

$$c_{ls}^{(0)} = \frac{2l+1}{2\pi(1+\delta_{0s})} \frac{(l-|s|)!}{(l+|s|)!} \int_0^{2\pi} \int_0^\pi u(R, \theta, \varphi) Y_l^s(\theta, \varphi) \sin \theta d\theta d\varphi,$$

$$c_{ls}^{(1)} = \frac{2l+1}{2\pi(1+\delta_{0s})} \frac{(l-|s|)!}{(l+|s|)!} \int_0^{2\pi} \int_0^\pi \frac{\partial u}{\partial r}(R, \theta, \varphi) Y_l^s(\theta, \varphi) \sin \theta d\theta d\varphi.$$

Substituting expansions (17) into formula (12) and using relations (16), as well as the orthogonality of the spherical harmonics Y_l^s , we can reduce the BGT boundary condition $B_m u = 0$ to the following system of algebraic equations with respect to the coefficients $c_{ls}^{(0)}$ and $c_{ls}^{(1)}$:

$$c_{ls}^{(1)} \alpha_m + c_{ls}^{(0)} \sum_{n=1}^{\lfloor \frac{m}{2} \rfloor} \beta_{m,n} [-l(l+1)]^n + c_{ls}^{(1)} \sum_{n=1}^{\lfloor \frac{m-1}{2} \rfloor} \gamma_{m,n} [-l(l+1)]^n + c_{ls}^{(0)} \left(\frac{1}{r} - ik \right) \alpha_m = 0, \tag{18}$$

$$l = 0, 1, 2, \dots, \quad s = -l, \dots, 0, \dots, l.$$

Note that, for sufficiently smooth u and $\frac{\partial u}{\partial r}$ at $r = R$, expansions (17) converge rapidly; namely, the remainder of the series behaves as l raised to the power of smoothness. Therefore, for the purpose of practical computing expansions (17) can be truncated at a finite l . This makes system (18) finite as well, see Section 4 for subsequent detail. We emphasize that equation (18) is of central importance as it converts the BGT ABC $B_m u = 0$ from its original variables to coefficients of the spectral expansion (17). It is the equivalent spectral form of the ABC (18) (truncated to a finite l) that we will actually implement numerically. Note also that while the transition from the conventional BGT ABC $B_m u = 0$ to its spectral form (18) can be interpreted as the replacement of a local ABC with a non-local one, it does not cause any difficulties in numerical implementation because the summation in (18) can always be truncated at a low value of l , see Sections 4.4 and 5.

In practice, we will also need to be able to evaluate $Y_l^s(\theta, \varphi)$ for a given pair of arguments (θ, φ) . The associated Legendre functions (15) can be efficiently computed with the help of the identity (see [21]):

$$\mathcal{P}_l^s(\cos\theta) = \sin^s \theta \mathcal{J}_{\ell-s}^{s,s}(\cos\theta),$$

where $\mathcal{J}_{\ell-s}^{s,s} = \mathcal{J}_{\ell-s}^{s,s}(x)$ is a normalized associated Jacobi polynomial defined via the following three-term recurrent relation:

$$\begin{aligned} \mathcal{J}_{-1}^{s,s}(x) &= 0, \\ \mathcal{J}_0^{s,s}(x) &= \sqrt{\frac{1}{2}} \prod_{j=1}^s \sqrt{1 + \frac{1}{2j}}, \\ \mathcal{J}_l^{s,s}(x) &= 2x\eta_{sl} \mathcal{J}_{l-1}^{s,s}(x) - \zeta_{sl} \mathcal{J}_{l-2}^{s,s}(x). \end{aligned}$$

The coefficients η_{sl} and ζ_{sl} in the last relation are given by $\eta_{sl} = \sqrt{\left(1 + \frac{s-1/2}{l}\right)\left(1 - \frac{s-1/2}{l+2s}\right)}$ and $\zeta_{sl} = \sqrt{\left(1 + \frac{4}{2l+2s-3}\right)\left(1 - \frac{1}{l}\right)\left(1 - \frac{1}{l+2s}\right)}$; one normally precomputes them for efficiency.

4. Difference potentials

The advantage of the BGT ABCs in the form (18) is that they require neither the approximation of high order derivatives on the grid nor the introduction of auxiliary variables. These boundary conditions still need to be combined with an interior solver. One natural way of doing that would be to use a volumetric spectral solver based on spherical harmonics (14). Otherwise, in the case of a general finite difference or finite element discretization of the Helmholtz equation inside Ω , the key question will be how to “reconcile” a node-based interior approximation built on a localized stencil with the global spectral representation (18) of the outer boundary conditions.

In the current paper, we employ the method of difference potentials (MDP) [20] for that purpose. It is a versatile technique that helps reduce the governing Helmholtz equation to an equivalent boundary operator equation, for which the operators are efficiently computed by high order finite differences on a volumetric grid. As such, the MDP can couple boundary conditions (18) with a high order accurate finite difference scheme inside the domain Ω . It is possible that alternative methods can also be developed that would offer similar capabilities. We, however, are not addressing this question and leave it for a future study.

To demonstrate our current concept yet keep the analysis as simple as possible, we only consider the inhomogeneous Helmholtz equation driven by a given source term. However, the same treatment of the artificial outer boundary will apply to a much broader variety of formulations, including single/multiple scattering, transmission, interfaces, etc., see [22–25].

4.1. Calderon’s operators

We are interested in solving the inhomogeneous Helmholtz equation on \mathbb{R}^3 :

$$\mathbf{L}u \equiv \frac{\partial^2 u}{\partial r^2} + \frac{2}{r} \frac{\partial u}{\partial r} + \frac{\Delta_{\theta,\varphi} u}{r^2} + k^2 u = f \tag{19}$$

subject to the Sommerfeld radiation condition at infinity:

$$r \left(\frac{\partial u}{\partial r} + iku \right) \rightarrow 0 \quad \text{as } r \rightarrow \infty. \tag{20}$$

The right-hand side f of equation (19) is assumed compactly supported.

Let $\Omega = \{(r, \theta, \varphi) | r \leq R, 0 \leq \theta \leq \pi, 0 \leq \varphi < 2\pi\}$ be the domain of interest where we would like to obtain the solution $u = u(r, \theta, \varphi)$ of problem (19), (20); Ω is a ball of radius R centered at the origin. We assume that $\text{supp } f \subset \Omega$. Let the sphere $\Gamma = \partial\Omega = \{(r, \theta, \varphi) | r = R, 0 \leq \theta \leq \pi, 0 \leq \varphi < 2\pi\}$ be the artificial outer boundary. Instead of solving problem (19), (20) on the entire \mathbb{R}^3 , we solve the Helmholtz equation (19) on the truncated domain Ω subject to the BGT ABC of order m at Γ :

$$B_m u \Big|_{r=R} = 0. \tag{21}$$

The operator B_m in (21) is defined by formula (12), and for the practical implementation we intend to use its spectral form (18).

Let Ω_0 be a larger cube that contains Ω , $\Omega_0 \supset \Omega$; hereafter, we will call Ω_0 the auxiliary domain. On this domain, consider an auxiliary problem (AP) for the Helmholtz equation (19):

$$\mathbf{L}u = g, \quad \mathbf{l}u|_{\partial\Omega_0} = 0, \tag{22}$$

where the boundary condition at $\partial\Omega_0$ should be chosen so that a unique solution u exists for any right-hand side g defined on Ω_0 . The specific form of this boundary condition is not important as long as it guarantees the unique solvability; examples can be found, e.g., in [22]. Let \mathbf{G} denote the Green's (i.e., inverse) operator that yields the solution of the AP (22):

$$u = \mathbf{G}g. \tag{23}$$

For an arbitrary function w on Ω_0 , define its vector trace on Γ :

$$\mathbf{Tr}_\Gamma w \stackrel{\text{def}}{=} \left(w, \frac{\partial w}{\partial r} \right) \Big|_{r=R}. \tag{24}$$

Consider a vector-function on Γ with two components: $\xi_\Gamma = (\xi_0, \xi_1)$. Take a sufficiently smooth w on Ω_0 , such that $\mathbf{l}w|_{\partial\Omega_0} = 0$ (see formula (22)) and $\mathbf{Tr}_\Gamma w = \xi_\Gamma$. A Calderon's potential with the density ξ_Γ on the domain Ω is defined by

$$\mathbf{P}_\Omega \xi_\Gamma \stackrel{\text{def}}{=} \mathbf{G} \left(\mathbf{L}w \Big|_{\Omega_0 \setminus \Omega} \right). \tag{25}$$

Hence, the potential (25) is a solution to the AP (22) for the right-hand side $g = \mathbf{L}w|_{\Omega_0 \setminus \Omega}$ obtained by applying the operator \mathbf{L} to w and truncating the result to $\Omega_0 \setminus \Omega$. By construction, the potential (25) satisfies a homogeneous Helmholtz equation on Ω : $\mathbf{L}\mathbf{P}_\Omega \xi_\Gamma = 0$.

The trace (24) of the potential (25) is known as Calderon's boundary projection:

$$\mathbf{P}_\Gamma \xi_\Gamma \stackrel{\text{def}}{=} \mathbf{Tr}_\Gamma \mathbf{P}_\Omega \xi_\Gamma. \tag{26}$$

One can show [20,26–29,23] that a given u provides a solution to equation (19) on Ω if and only if its trace (24), $\mathbf{Tr}_\Gamma u = \xi_\Gamma$, satisfies the Calderon boundary equation with projection (BEP):

$$\mathbf{P}_\Gamma \xi_\Gamma + \mathbf{Tr}_\Gamma \mathbf{G}f = \xi_\Gamma. \tag{27}$$

The boundary operator equation (27) on Γ is equivalent to the differential equation (19) on Ω . Equation (27) is not tied to any boundary conditions. A boundary condition, in particular, a BGT ABC, needs to be added to equation (27) to form a combined system of boundary equations on Γ .

Since we have introduced the notation $\xi_\Gamma = (\xi_0, \xi_1)$ for traces, it is convenient to recast the BGT ABC (21) as follows [cf. formula (12)]:

$$\alpha_m \xi_1 + \sum_{n=1}^{\lfloor \frac{m}{2} \rfloor} \beta_{m,n} \Delta_{\theta,\varphi}^n \xi_0 + \sum_{n=1}^{\lfloor \frac{m-1}{2} \rfloor} \gamma_{m,n} \Delta_{\theta,\varphi}^n \xi_1 + \left(\frac{1}{r} - ik \right) \alpha_m \xi_0 = 0. \tag{28}$$

The system of equations (27), (28), which is formulated only at the boundary Γ with respect to the unknown ξ_Γ , is equivalent to problem (19), (20) on Ω . Once ξ_Γ has been determined by solving equations (27), (28), the solution u on Ω is given by the sum of the Calderon potential (25) with the density ξ_Γ and the inhomogeneous term:

$$u = \mathbf{P}_\Omega \xi_\Gamma + \mathbf{G}f. \tag{29}$$

Again, we refer the reader to [20,26–29,23] for detail.

Let us now expand the components $\xi_0 = \xi_0(\theta, \varphi)$ and $\xi_1 = \xi_1(\theta, \varphi)$ of ξ_Γ in spherical harmonics [cf. formulae (17)]:

$$\xi_0(\theta, \varphi) = \sum_{l,s} c_{ls}^{(0)} Y_l^s(\theta, \varphi), \tag{30a}$$

$$\xi_1(\theta, \varphi) = \sum_{l,s} c_{ls}^{(1)} Y_l^s(\theta, \varphi). \tag{30b}$$

Substituting expansions (30) into equations (27) and (28), we obtain a system of equations with respect to the coefficients $c_{ls}^{(0)}$ and $c_{ls}^{(1)}$. In doing so, the BGT boundary condition (28) transforms into (18), as expected. A constructive discretization of the boundary problem (27), (28) will be based on truncated expansions (30).

4.2. Discrete Calderon's operators

Let \mathbb{N}_0 be a 3D uniform Cartesian grid on Ω_0 ; the finite difference solution $u^{(h)}$ of the Helmholtz equation will be defined on \mathbb{N}_0 . Similarly, let \mathbb{M}_0 be another Cartesian grid on Ω_0 ; the discrete right-hand side $f^{(h)}$ will be defined on \mathbb{M}_0 . Introduce the compact sixth order accurate finite difference scheme of [19] that approximates the Helmholtz equation on these grids:

$$\mathbf{L}^{(h)} u^{(h)} = \mathbf{B}^{(h)} f^{(h)}. \tag{31}$$

Note that compact high order differencing normally results in two different operators, $\mathbf{L}^{(h)}$ and $\mathbf{B}^{(h)}$, applied to the left-hand side and right-hand side of the equation, respectively.

Along with (31), consider a more general formulation [cf. formula (22)]:

$$\mathbf{L}^{(h)} u^{(h)} = g^{(h)}, \quad \mathbf{I}^{(h)} u^{(h)} \Big|_{\partial\Omega_0} = 0, \tag{32}$$

where $g^{(h)}$ is an arbitrary right-hand side on \mathbb{M}_0 . Similarly to (22), we are assuming that the discrete boundary condition at $\partial\Omega_0$ guarantees the existence and uniqueness of the solution $u^{(h)}$ for any $g^{(h)}$. The finite difference problem (32) will be referred to as the difference AP. Its solution can be written as

$$u^{(h)} = \mathbf{G}^{(h)} g^{(h)}, \tag{33}$$

where $\mathbf{G}^{(h)}$ is the inverse to $\mathbf{L}^{(h)}$ subject to the chosen boundary condition $\mathbf{I}^{(h)} u^{(h)} \Big|_{\partial\Omega_0} = 0$ (see formula (32)), i.e., a discrete Green's operator.

Let \mathbb{N}_m be the stencil of the finite difference operator $\mathbf{L}^{(h)}$ centered at a given node $m \in \mathbb{M}_0$. For the compact sixth order accurate scheme of [19], the stencil \mathbb{N}_m is $3 \times 3 \times 3$. Split the grid \mathbb{M}_0 into two non-overlapping subsets:

$$\mathbb{M}_0 = \mathbb{M}^+ \cup \mathbb{M}^-, \quad \text{where } \mathbb{M}^+ = \mathbb{M}_0 \cap \bar{\Omega} \text{ and } \mathbb{M}^- = \mathbb{M}_0 \setminus \mathbb{M}^+.$$

Consider two subsets of the grid \mathbb{N}_0 :

$$\mathbb{N}^+ = \bigcup_{m \in \mathbb{M}^+} \mathbb{N}_m \quad \text{and} \quad \mathbb{N}^- = \bigcup_{m \in \mathbb{M}^-} \mathbb{N}_m.$$

Unlike \mathbb{M}^+ and \mathbb{M}^- , these two subsets do overlap, and we call their intersection the grid boundary:

$$\gamma = \mathbb{N}^+ \cap \mathbb{N}^-.$$

It is a multi-layer fringe of nodes of the grid \mathbb{N}_0 that straddles the continuous boundary Γ .

Let ξ_γ be a grid function defined on γ . We can extend it by zero to the entire grid \mathbb{N}_0 :

$$w^{(h)} \Big|_n = \begin{cases} \xi_\gamma \Big|_n, & n \in \gamma, \\ 0, & n \in \mathbb{N}_0 \setminus \gamma. \end{cases}$$

Then, we define a discrete Calderon's potential (difference potential) with the density ξ_γ [cf. formula (25)]:

$$\mathbf{P}_{\mathbb{N}^+ \xi_\gamma} \stackrel{\text{def}}{=} \mathbf{G}^{(h)} \left(\mathbf{L}^{(h)} w^{(h)} \Big|_{\mathbb{M}^-} \right). \tag{34}$$

On the right-hand side of (34), the discrete Green's operator $\mathbf{G}^{(h)}$ of (33) acts on the result of application of the operator $\mathbf{L}^{(h)}$ to $w^{(h)}$ truncated to the grid \mathbb{M}^- . In other words, the potential $\mathbf{P}_{\mathbb{N}^+ \xi_\gamma}$ is a solution to the difference AP (32) for the right-hand side $g^{(h)} = \mathbf{L}^{(h)} w^{(h)} \Big|_{\mathbb{M}^-}$. By design, the potential (34) satisfies the homogeneous difference equation $\mathbf{L}^{(h)} (\mathbf{P}_{\mathbb{N}^+ \xi_\gamma}) = 0$ on \mathbb{M}^+ .

The trace of a given grid function $w^{(h)}$ on the grid boundary γ will be its plain restriction:

$$\mathbf{Tr}_\gamma w^{(h)} \stackrel{\text{def}}{=} w^{(h)} \Big|_\gamma. \tag{35}$$

The trace (35) of the potential (34) yields a difference Calderon's projection [cf. formula (26)]:

$$\mathbf{P}_\gamma \xi_\gamma \stackrel{\text{def}}{=} \mathbf{Tr}_\gamma \mathbf{P}_{\mathbb{N}^+ \xi_\gamma} = \mathbf{Tr}_\gamma \mathbf{G}^{(h)} \left(\mathbf{L}^{(h)} \xi_\gamma \Big|_{\mathbb{M}^-} \right). \tag{36}$$

A grid function $u^{(h)}$ defined on \mathbb{N}^+ provides a solution to the finite difference Helmholtz equation (31) (i.e., satisfies equation (31) everywhere on \mathbb{M}^+) if and only if its trace $\xi_\gamma = \mathbf{Tr}_\gamma u^{(h)}$ defined by (35) satisfies the discrete BEP (or difference BEP) [cf. equation (27)]:

$$\mathbf{P}_\gamma \xi_\gamma + \mathbf{Tr}_\gamma \mathbf{G}^{(h)} \mathbf{B}^{(h)} f^{(h)} = \xi_\gamma. \tag{37}$$

In other words, similarly to the continuous BEP (27), the discrete BEP (37) equivalently reduces the finite difference Helmholtz equation (31) from the domain to the grid boundary γ . As in the continuous case, the discrete BEP (37) is written independently of any specific boundary conditions. A spectral boundary condition (28) is to be added to equation (37) to form a combined system.

Note that, the BEP (27) is formulated for the continuous function ξ_Γ , while the difference BEP (37) is formulated for the grid function ξ_γ (essentially, a vector of finite dimension). The same is true for the potentials $\mathbf{P}_\Omega \xi_\Gamma$ of (25) and $\mathbf{P}_{\mathbb{N}+\xi_\gamma}$ of (34), respectively. Whereas the continuous and discrete Calderon’s operators are introduced independently, the relation between them is of central importance. Specifically, one can show that the difference potential (34) approximates the continuous potential (25) with the design order of accuracy of the scheme as long as the following two conditions hold. The solution to the difference AP (33) must approximate the solution to the continuous AP (23) with the same accuracy. Besides, the discrete density ξ_γ must be obtained from the continuous density ξ_Γ by a special extension procedure: $\xi_\gamma = \mathbf{E}\mathbf{x}\xi_\Gamma$, described in Section 4.3.

4.3. Extension operator

Let $\xi_\Gamma = (\xi_0, \xi_1)|_\Gamma$ be specified on $\Gamma = \partial\Omega = \{(r, \theta, \varphi) | r = R, 0 \leq \theta \leq \pi, 0 \leq \varphi < 2\pi\}$ so that $\xi_0 = \xi_0(\theta, \varphi)$ and $\xi_1 = \xi_1(\theta, \varphi)$. In the vicinity of Γ , we define a new smooth function $v = v(r, \theta, \varphi)$ by means of the Taylor formula:

$$v(r, \theta, \varphi) = v(R, \theta, \varphi) + \sum_{j=1}^J \frac{1}{j!} \frac{\partial^j v(R, \theta, \varphi)}{\partial r^j} h^j, \tag{38}$$

where $h = r - R$. For our subsequent derivations, we will need to take $J = 6$. Otherwise, the general choice of J in formula (38) is discussed toward the end of this section. The zeroth and first order derivatives on the right-hand side of (38) are obtained by requiring that $\mathbf{Tr}_\Gamma v = \xi_\Gamma$:

$$v(R, \theta, \varphi) = \xi_0(\theta, \varphi) \quad \text{and} \quad \frac{\partial v(R, \theta, \varphi)}{\partial r} = \xi_1(\theta, \varphi). \tag{39}$$

All higher order derivatives in formula (38) are obtained by differentiating equation (19) applied to v . Up to the derivative of order six, this yields:

$$\begin{aligned} \frac{\partial^2 v}{\partial r^2} &= f - \frac{2}{r} \frac{\partial v}{\partial r} - \left(\frac{\Delta_{\theta, \varphi}}{r^2} + k^2 \right) v, \\ \frac{\partial^3 v}{\partial r^3} &= f_r - \frac{2}{r} \frac{\partial^2 v}{\partial r^2} + \frac{2\Delta_{\theta, \varphi} v}{r^3} - \left(\frac{\Delta_{\theta, \varphi}}{r^2} - \frac{2}{r^2} + k^2 \right) \frac{\partial v}{\partial r}, \\ \frac{\partial^4 v}{\partial r^4} &= f_{rr} - \frac{2}{r} \frac{\partial^3 v}{\partial r^3} - \left(\frac{\Delta_{\theta, \varphi}}{r^2} - \frac{4}{r^2} + k^2 \right) \frac{\partial^2 v}{\partial r^2} + \frac{4(\Delta_{\theta, \varphi} - 1)}{r^3} \frac{\partial v}{\partial r} - \frac{6\Delta_{\theta, \varphi} v}{r^4}, \\ \frac{\partial^5 v}{\partial r^5} &= f_{rrr} - \frac{2}{r} \frac{\partial^4 v}{\partial r^4} - \left(\frac{\Delta_{\theta, \varphi}}{r^2} - \frac{6}{r^2} + k^2 \right) \frac{\partial^3 v}{\partial r^3} + \frac{6(\Delta_{\theta, \varphi} - 2)}{r^3} \frac{\partial^2 v}{\partial r^2} - \frac{6(3\Delta_{\theta, \varphi} - 2)}{r^4} \frac{\partial v}{\partial r} + \frac{24\Delta_{\theta, \varphi} v}{r^5}, \\ \frac{\partial^6 v}{\partial r^6} &= f_{rrrr} - \frac{2}{r} \frac{\partial^5 v}{\partial r^5} - \left(\frac{\Delta_{\theta, \varphi}}{r^2} - \frac{8}{r^2} + k^2 \right) \frac{\partial^4 v}{\partial r^4} + \frac{8(\Delta_{\theta, \varphi} - 3)}{r^3} \frac{\partial^3 v}{\partial r^3} \\ &\quad - \frac{12(3\Delta_{\theta, \varphi} - 4)}{r^4} \frac{\partial^2 v}{\partial r^2} + \frac{48(2\Delta_{\theta, \varphi} - 1)}{r^5} \frac{\partial v}{\partial r} - \frac{120\Delta_{\theta, \varphi} v}{r^6}. \end{aligned}$$

In practice, we will use formula (38) only in the case where ξ_0 and ξ_1 are spherical harmonics, e.g., $\xi_0(\theta, \varphi) = Y_l^s$ and $\xi_1(\theta, \varphi) = Y_l^s$. Then, we won’t need to evaluate the Beltrami operator $\Delta_{\theta, \varphi}$ applied to v and its radial derivatives. Instead, we employ formula (16): $\Delta_{\theta, \varphi} Y_l^s = -l(l+1)Y_l^s$. For the radial derivatives $\frac{\partial^2 v}{\partial r^2}$ and $\frac{\partial^3 v}{\partial r^3}$, this yields:

$$\begin{aligned} \frac{\partial^2 v}{\partial r^2} &= f - \frac{2}{r} \frac{\partial v}{\partial r} + \left(\frac{l(l+1)}{r^2} - k^2 \right) v, \\ \frac{\partial^3 v}{\partial r^3} &= f_r - \frac{2}{r} \frac{\partial^2 v}{\partial r^2} - \frac{2l(l+1)v}{r^3} + \left(\frac{l'(l'+1)}{r^2} + \frac{2}{r^2} - k^2 \right) \frac{\partial v}{\partial r}. \end{aligned}$$

Evaluation of $\frac{\partial^4 v}{\partial r^4}$, $\frac{\partial^5 v}{\partial r^5}$, and $\frac{\partial^6 v}{\partial r^6}$ requires the application of $\Delta_{\theta, \varphi}$ (and its powers) to higher order radial derivatives of v (beyond first order), which, in turns, entails substitution of the previously obtained expressions:

$$\begin{aligned} \Delta_{\theta,\varphi} \frac{\partial^2 v}{\partial r^2} &= \Delta_{\theta,\varphi} f - \Delta_{\theta,\varphi} \frac{2}{r} \frac{\partial v}{\partial r} + \left(\frac{l(l+1)}{r^2} - k^2 \right) \Delta_{\theta,\varphi} v \\ &= \Delta_{\theta,\varphi} f + \frac{2l'(l'+1)}{r} \frac{\partial v}{\partial r} - \left(\frac{l(l+1)}{r^2} - k^2 \right) l(l+1)v, \\ \Delta_{\theta,\varphi}^2 \frac{\partial^2 v}{\partial r^2} &= \Delta_{\theta,\varphi}^2 f + \frac{2(l'(l'+1))^2}{r} \frac{\partial v}{\partial r} - \left(\frac{l(l+1)}{r^2} - k^2 \right) l^2(l+1)^2 v, \\ \Delta_{\theta,\varphi} \frac{\partial^3 v}{\partial r^3} &= \Delta_{\theta,\varphi} f_r - \Delta_{\theta,\varphi} \frac{2}{r} \frac{\partial^2 v}{\partial r^2} - \frac{2l^2(l+1)^2 v}{r^3} + \left(\frac{l'(l'+1)}{r^2} + \frac{2}{r^2} - k^2 \right) l'(l'+1) \frac{\partial v}{\partial r}, \\ \Delta_{\theta,\varphi} \frac{\partial^4 v}{\partial r^4} &= \Delta_{\theta,\varphi} f_{rr} - \Delta_{\theta,\varphi} \frac{2}{r} \frac{\partial^3 v}{\partial r^3} - \left(\frac{\Delta_{\theta,\varphi}}{r^2} - \frac{4}{r^2} + k^2 \right) \Delta_{\theta,\varphi} \frac{\partial^2 v}{\partial r^2} + \frac{4(\Delta_{\theta,\varphi}^2 - \Delta_{\theta,\varphi})}{r^3} \frac{\partial v}{\partial r} + \frac{6l(l+1)v}{r^4} \\ &= \Delta_{\theta,\varphi} f_{rr} - \Delta_{\theta,\varphi} \frac{2}{r} \frac{\partial^3 v}{\partial r^3} + \left(\frac{4}{r^2} - k^2 \right) \Delta_{\theta,\varphi} \frac{\partial^2 v}{\partial r^2} - \frac{\Delta_{\theta,\varphi}^2}{r^2} \frac{\partial^2 v}{\partial r^2} \\ &\quad + \frac{4((l'(l'+1))^2 + l'(l'+1))}{r^3} \frac{\partial v}{\partial r} + \frac{6l(l+1)v}{r^4}. \end{aligned}$$

Finally, recalling that $J = 6$, we arrive at

$$\begin{aligned} v &= \frac{h^6}{720r^4} \Delta_{\theta,\varphi}^2 f + \frac{h^6}{720} f_{rrrr} - \frac{(h-3r)h^5}{360r} f_{rrr} \\ &\quad - \Delta_{\theta,\varphi} \left(\frac{h^6}{720r^2} f_{rr} - \frac{(2h-r)h^5}{120r^3} f_r - \frac{h^4}{360r^2} \left(h^2k^2 - \frac{44h^2 - 30hr + 15r^2}{r^2} \right) f \right) \\ &\quad + \frac{h^4}{120} \left(\frac{2h(h-r) + 5r^2}{r^2} - \frac{h^2k^2}{6} \right) f_{rr} + \frac{h^3}{12} \left(\frac{h(hr-r^2-h^2)}{r^3} + \frac{h^2k^2(4h-6r)}{60r} + 2 \right) f_r \\ &\quad + \frac{h^2}{720} \left(h^4k^4 + 360 + \frac{240h(h-r)(h^2+r^2)}{r^4} - \frac{6h^2k^2(4h^2-4hr+5r^2)}{r^2} \right) f \\ &\quad + A\xi_0 + B\xi_1, \end{aligned} \tag{40}$$

where

$$\begin{aligned} A &= 1 - \frac{h^6l^3(l+1)^3}{720r^6} + (l(l+1))^2 \frac{h^4}{120} \left(\frac{h^2k^2}{2r^4} - \frac{59h^2 - 36hr + 15r^2}{3r^6} \right) \\ &\quad + \frac{h^2l(l+1)}{120} \left(\frac{h^4k^4}{2r^2} - \frac{h^2k^2(21h^2 - 16hr + 10r^2)}{r^4} + \frac{100h^4 - 96h^3r + 90h^2r^2 - 80hr^3 + 60r^4}{r^6} \right) \\ &\quad - \frac{h^2k^2}{720} \left(h^4k^4 - \frac{6h^2k^2(4h^2 - 4hr + 5r^2)}{r^2} + \frac{240h(h-r)(h^2+r^2)}{r^4} + 360 \right) \end{aligned}$$

and

$$\begin{aligned} B &= \frac{(r-h)h^5k^4}{120r} - \frac{(r-h)(h^2+r^2)h^3k^2}{6r^3} + \frac{(l'(l'+1))^2(r-3h)h^5}{120r^5} \\ &\quad + \frac{-rh^6 + r^2h^5 - r^3h^4 + r^4h^3 - r^5h^2 + r^6h}{r^6} \\ &\quad + l'(l'+1) \frac{h^3}{60r^3} \left(\frac{37h^3 - 29h^2r + 20hr^2 - 10r^3}{r^2} + h^2k^2(r-2h) \right). \end{aligned}$$

Once we have obtained the function $v = v(r, \theta, \varphi)$ of (38) in the form (40) for a given $\xi_\Gamma = (\xi_0, \xi_1)$ (see formula (39)), we can evaluate it at the nodes of the grid boundary γ . This yields the equation-based extension of ξ_Γ from Γ to γ :

$$\xi_\gamma = \mathbf{E} \mathbf{x} \xi_\Gamma \stackrel{\text{def}}{=} v(r, \theta, \varphi) \Big|_\gamma. \tag{41}$$

As shown in [30],¹ if the upper limit of summation J in formula (38) is chosen as the sum of the order of accuracy of the scheme (31) and the order of the differential operator \mathbf{L} , and the continuous and discrete densities are related via the equation-based extension (41), then the difference potential (34) will approximate the continuous potential (25) with the same order of accuracy. In our case, the scheme is sixth order accurate and the Helmholtz equation (19) is a second order differential equation. Hence, we should have chosen $J = 8$. As however, we have seen in our previous computations [29,22,23] (and as has been repeatedly observed by others), the theoretical estimates of [30] are not sharp, and it is sufficient to take J equal to the desired order of accuracy. Therefore, we are taking $J = 6$ hereafter. Equation (41) plays a pivotal role as it basically allows us to substitute continuous unknowns defined at the boundary Γ into the discrete BEP (37).

4.4. Discrete system of equations

We would like to find a solution ξ_Γ to the system of boundary equations (27), (28) that, in turn, is equivalent to the Helmholtz problem (19), (21). To approximate ξ_Γ , we truncate the series (30) at a finite $l = L$:

$$\xi_0(\theta, \varphi) = \sum_{l=0}^L \sum_{s=-l}^l c_{ls}^{(0)} Y_l^s(\theta, \varphi), \tag{42a}$$

$$\xi_1(\theta, \varphi) = \sum_{l=0}^L \sum_{s=-l}^l c_{ls}^{(1)} Y_l^s(\theta, \varphi). \tag{42b}$$

For convenience, we also define the two-dimensional vector-functions on Γ that form a basis of finite dimension:

$$\begin{aligned} \boldsymbol{\psi}_{ls}^{(0)} &= (Y_l^s, 0) \text{ and } \boldsymbol{\psi}_{ls}^{(1)} = (0, Y_l^s), \\ l &= 0, \dots, L, \quad s = -l, \dots, 0, \dots, l. \end{aligned} \tag{43}$$

Then, expansions (42a) and (42b) can be combined into one expansion for $\xi_\Gamma = (\xi_0, \xi_1)$:

$$\xi_\Gamma = \sum_{l=0}^L \sum_{s=-l}^l c_{ls}^{(0)} \boldsymbol{\psi}_{ls}^{(0)} + c_{ls}^{(1)} \boldsymbol{\psi}_{ls}^{(1)}. \tag{44}$$

Rapid convergence of the series (30) implies that for sufficiently smooth solutions the representation (44) that employs a basis of spherical harmonics that has finite dimension, see (43), will provide adequate accuracy already for modest values of L .

Instead of substituting ξ_Γ of (44) directly into the continuous BEP (27), we recall that the discrete Calderon operators approximate continuous Calderon’s operators provided that the densities satisfy (41), and rather use the difference BEP (37). The advantage of using the difference BEP (37) is that there is a constructive procedure for computing the operators involved – the AP (32).

Applying the extension operator (41) to ξ_Γ of (44), we obtain:

$$\xi_\gamma = \mathbf{E}\mathbf{x}\xi_\Gamma = \sum_{l=0}^L \sum_{s=-l}^l c_{ls}^{(0)} \mathbf{E}\mathbf{x}\boldsymbol{\psi}_{ls}^{(0)} + c_{ls}^{(1)} \mathbf{E}\mathbf{x}\boldsymbol{\psi}_{ls}^{(1)}. \tag{45}$$

Thus, we will be looking for a solution ξ_γ to the discrete BEP (37) in the form (45).

Let $\mathbf{Q}_\gamma = \mathbf{P}_\gamma - \mathbf{I}_\gamma$ so that the BEP (37) can be recast as

$$\mathbf{Q}_\gamma \xi_\gamma = -\mathbf{T}\mathbf{r}_\gamma \mathbf{G}^{(h)} \mathbf{B}^{(h)} f^{(h)}. \tag{46}$$

Substituting ξ_γ of (45) into (46), we have:

$$\sum_{l=0}^L \sum_{s=-l}^l c_{ls}^{(0)} \mathbf{Q}_\gamma \mathbf{E}\mathbf{x}\boldsymbol{\psi}_{ls}^{(0)} + c_{ls}^{(1)} \mathbf{Q}_\gamma \mathbf{E}\mathbf{x}\boldsymbol{\psi}_{ls}^{(1)} = -\mathbf{T}\mathbf{r}_\gamma \mathbf{G}^{(h)} \mathbf{B}^{(h)} f^{(h)}. \tag{47}$$

Formula (47) defines a system of linear algebraic equations with respect to the coefficients $c_{ls}^{(0)}$ and $c_{ls}^{(1)}$, $l = 0, \dots, L$, $s = -l, \dots, 0, \dots, l$. Note that, the application of the projection \mathbf{Q}_γ to the extended basis functions of (43), $\mathbf{E}\mathbf{x}\boldsymbol{\psi}_{ls}^{(0)}$ and $\mathbf{E}\mathbf{x}\boldsymbol{\psi}_{ls}^{(1)}$, requires one solution of the difference AP (32) per basis function. This computation needs to be conducted only once. It does not need to be repeated, if, for example, the right-hand side $f^{(h)}$ subsequently changes, see (47).

¹ See [20, Part III, Section 1.4] and [31] for further detail and [29] for the specific account of compact schemes.

We emphasize that system (47) has been derived from the difference BEP (37) and as such, it remains a system of difference equations on the grid. However, the unknowns in system (47) are the coefficients of the expansion of ξ_Γ with respect to the continuous basis (43). The dimension of this basis is finite; it yields the number of unknowns in system (47). The number of equations in this system is equal to the number of nodes $|\gamma|$ in the grid boundary γ .

System (47) still needs to be supplemented by the BGT boundary condition on Γ . As the unknowns in (47) are coefficients of an expansion with respect to the basis (43), it is both natural and convenient to combine (47) with the spectral form of the BGT boundary condition (18) truncated to the same finite value of $l = L$ as in formulae (42):

$$c_{l_s}^{(1)} \alpha_m + c_{l_s}^{(0)} \sum_{n=1}^{\lfloor \frac{m}{2} \rfloor} \beta_{m,n} [-l(l+1)]^n + c_{l_s}^{(1)} \sum_{n=1}^{\lfloor \frac{m-1}{2} \rfloor} \gamma_{m,n} [-l(l+1)]^n + c_{l_s}^{(0)} \left(\frac{1}{r} - ik \right) \alpha_m = 0, \quad (48)$$

$$l = 0, 1, 2, \dots, L, \quad s = -l, \dots, 0, \dots, l.$$

Equations (47) coupled with (48) form the complete system of linear algebraic equations with respect to the unknown coefficients $c_{l_s}^{(0)}$ and $c_{l_s}^{(1)}$, $l = 0, \dots, L$, $s = -l, \dots, 0, \dots, l$. In this combined system, equation (47) stems from the Helmholtz equation and equation (48) represents the BGT ABC. System (47), (48) is to be solved in the sense of least squares (by means of QR factorization). Once the coefficients have been determined, one can obtain the discrete density ξ_γ according to (45) and reconstruct the solution on the domain Ω (more precisely, on the grid \mathbb{N}^+) in the form of a difference potential with the density ξ_γ plus the inhomogeneous term [cf. formula (29)]:

$$u^{(h)} = \mathbf{P}_{\mathbb{N}^+} \xi_\gamma + \mathbf{G}^{(h)} \mathbf{B}^{(h)} f^{(h)}. \quad (49)$$

It only remains to discuss the choice of L that provides the upper limit of summation in (42). As the solution of the Helmholtz equation is eventually obtained on the grid, see formula (49), and is supposed to converge with the design accuracy of the finite difference scheme (sixth order accuracy in the case of scheme [19]), it is sufficient to choose L so that the accuracy of the truncated expansion (44) at the boundary will be at least as good as the accuracy that one would expect to obtain on the finest grid for a given range of simulations. For smooth solutions that facilitate rapid convergence of expansion (30), it turns out that the required values of L are fairly small. The specific value of L that we used in our simulations is provided in Section 5.1.

Moreover, as L is small, so is the horizontal dimension of the matrix of system (47), (48) that is solved by QR factorization. As such, the cost of solving system (47), (48) in the sense of least squares appears insignificant. A more substantial contribution to the overall cost comes from the computation of column vectors $\mathbf{Q}_\gamma \mathbf{E} \mathbf{x} \psi_{l_s}^{(0)}$ and $\mathbf{Q}_\gamma \mathbf{E} \mathbf{x} \psi_{l_s}^{(1)}$ that appear on the left hand side of equation (47). To compute each of those column vectors, one needs to apply the projection \mathbf{Q}_γ , i.e., solve the difference AP (32) once. This procedure, however, can be very efficiently parallelized, because different column vectors correspond to different basis functions $\psi_{l_s}^{(0)}$ and $\psi_{l_s}^{(1)}$ that are completely independent from one another.

5. Results

5.1. Computational setting

In the subsequent numerical simulations, we solve the Helmholtz equation (19) with constant wavenumber k . The computational domain Ω is a sphere of radius R centered at the origin. It is terminated by the BGT ABCs (21) of order 1 through 6. To investigate how the performance of the BGT ABCs in the truncated spectral form (48) depends on the size of Ω , we take $k = 1$ and consider five different values of the radius: $R = 1, 2, 4, 8$, and 16 . To see how the performance of the ABCs (48) is affected by the wavenumber k or, equivalently, the wavelength $\lambda = 2\pi/k$, we take $R = 1$ and consider six different values of the wavenumber: $k = 1, 2, 4, 8, 16$, and 32 . Given that the BGT ABC $B_m u = 0$ cancels out m leading terms in the far-field expansion of the solution (5), the reflection error will be determined by the largest remaining term of the expansion, which is $\propto (kR)^{-m-1}$. Thus, we expect that for a fixed order m of the boundary condition, the error will decrease as R increases and it will also decrease as k increases. At the same time, for a fixed value of kR , the error is expected to decrease as the order m of the ABC increases.

The auxiliary domain Ω_0 is a larger cube $2.8R \times 2.8R \times 2.8R$. It is discretized by a sequence of Cartesian grids $2^d \times 2^d \times 2^d$ with $d = 4, 5, 6, 7, 8$, and 9 , which allow us to study the grid convergence. Since the sizes of Ω and Ω_0 are related, we can maintain similar grid sizes h across different domains. This, in turn, yields similar values of the discretization error and thus allows a valid comparison.

The number of basis functions for MDP (see formula (42)) is taken as $L = 20$ in all our computations. This value of L proves sufficient for having the accuracy of the truncated expansion at the boundary Γ exceed the accuracy of the discrete approximation even on the finest grid.

5.2. Test solutions

We analyze source terms f of two types for the Helmholtz equation (19) – monopole and dipole. To avoid symmetries that may reduce the generality and thus misrepresent the performance of the ABCs, both sources are shifted off center with

respect to the spherical computational domain Ω . Moreover, as δ -functions cannot be directly approximated on the grid, the singularity of each test solution is smoothed out.

Let $r_0(x, y, z) = \sqrt{(x - x_0)^2 + (y - y_0)^2 + (z - z_0)^2}$. A monopole centered at (x_0, y_0, z_0) is given by

$$u(x, y, z) = \frac{e^{ikr_0(x, y, z)}}{r_0(x, y, z)}. \tag{50}$$

To remove its singularity near the center, we multiply (50) by a smooth step function

$$S_n^\alpha(r) = \begin{cases} \left(\frac{r}{\alpha}\right)^{n+1} \sum_{k=0}^n \binom{n+k}{n} \binom{2n+1}{n-k} \left(-\frac{r}{\alpha}\right)^k, & 0 \leq r < \alpha, \\ 1, & r \geq \alpha, \end{cases} \tag{51}$$

for $n = 7$ and $\alpha = \frac{1}{2}$, which yields:

$$u_m(x, y, z) = u(x, y, z) \cdot S_7^{\frac{1}{2}}(r_0(x, y, z)). \tag{52}$$

The function $S_7^{\frac{1}{2}}$ of (51) is a polynomial of degree 15 on the interval $[0, \alpha]$ that has zero derivatives of order up to 7 at both endpoints. Given that the singularity in (50) is first order, the product (52) has bounded derivatives of order at least 6 everywhere. Moreover, for $r_0(x, y, z) \geq \alpha$ the function u_m defined by (52) coincides with u of (50). In other words, sufficiently far away from the center u_m is a plain monopole solution. Therefore, the application of the Helmholtz operator \mathbf{L} of (19) to u_m of (52) yields a bounded smooth source term $f_m = \mathbf{L}u_m$ that is compactly supported on the ball of radius $\alpha = \frac{1}{2}$ centered at (x_0, y_0, z_0) . This source term provides the right-hand side to the Helmholtz equation (19), for which we solve this equation numerically.

In addition to the monopole, we use a smoothed out dipole:

$$u_d(x, y, z) = \frac{\partial u(x, y, z)}{\partial x} \cdot S_9^{\frac{1}{2}}(r_0(x, y, z)). \tag{53}$$

The corresponding source term is also obtained by applying the Helmholtz operator: $f_d = \mathbf{L}u_d$.

In all numerical simulations reported in Sections 5.3 and 5.4, we take $(x_0, y_0, z_0) = (0.1, 0.1, 0.1)$.

5.3. Monopole

5.3.1. Variation of R for a fixed k

In Figs. 1 and 2, we show the grid convergence of the proposed algorithm in the case of a monopole source, i.e., the source term $f_m = \mathbf{L}u_m$ in the Helmholtz equation (19), where u_m is given by (52). Every plot in these figures uses log-log scale and shows the maximum norm of the error across the domain Ω (i.e., across the grid \mathbb{N}^+) as a function of the grid dimension or, more precisely, as a function of the reciprocal size $1/h$ of the Cartesian grid that we use for discretization of the problem (see Sections 4.2 and 5.1).

Individual panels in Fig. 1, i.e., Figs. 1a through 1e, correspond to different sizes of the spherical domain Ω , i.e., different values of its radius: $R = 1, 2, 4, 8,$ and 16 , while individual graphs in each panel correspond to the BGT ABCs of order 1 to 6. One can clearly see that for each value of R the scheme converges with the design sixth order accuracy as the grid is refined (i.e., as $1/h$ increases). However, at some point the grid convergence stops and the error profiles become flat. This happens when the discretization error on the grid becomes smaller than the reflection error from the artificial outer boundary. The latter depends on the order of the BGT ABC rather than the grid size. Therefore, for a fixed R the higher the order of the ABC the further down the discretization error goes before the reflection error starts to dominate the numerical solution. At the same time, for larger values of R the reflection error gets smaller for ABCs of all orders. Thus, for example in Fig. 1d ($R = 8$) only the lowest order ABC – BGT1 – shows some slowdown of grid convergence for large values of $1/h$, while in Fig. 1e ($R = 16$) the reflection error for BGT ABCs of all orders is already sufficiently small so that the overall error is dominated by the discretization error for every grid that we have used.

Fig. 2 represents the same data as Fig. 1, but arranged differently. Individual panels in Fig. 2, i.e., Figs. 2a through 2f, correspond to BGT ABCs of order 1 through 6, respectively, while individual curves in each panel show the grid convergence on spherical computational domains Ω with the radius $R = 1, 2, 4, 8,$ and 16 . One can see that for a given order of the ABC, the scheme converges with the design accuracy until the convergence ceases. This happens when the reflection error becomes dominant. The specific point of transition depends on the size of Ω – the larger the R the later it occurs. Moreover, as the reflection error decreases when the order of the boundary condition increases, for higher order ABCs – BGT4 to BGT6 – one can observe a slowdown of grid convergence only for the smallest computational domain, $R = 1$.

The actual values of the error, i.e., the numerical data that gave rise to the plots in Figs. 1 and 2, are presented in Tables 1 and 2. In addition, Tables 1 and 2 show the calculated rates of grid convergence that corroborate the sixth order accuracy of the scheme for those ranges of parameters where the discretization error dominates over the reflection error. For reference

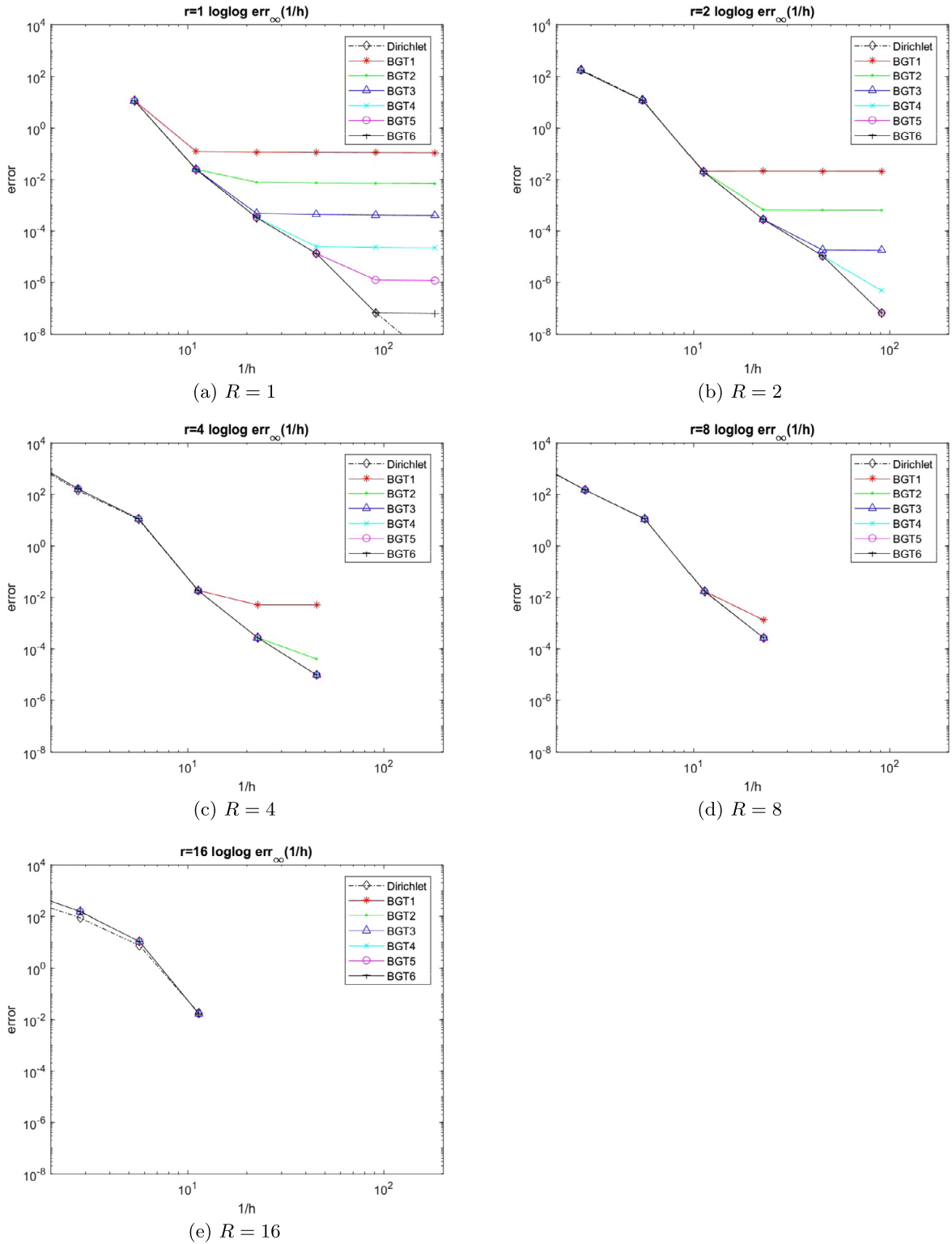
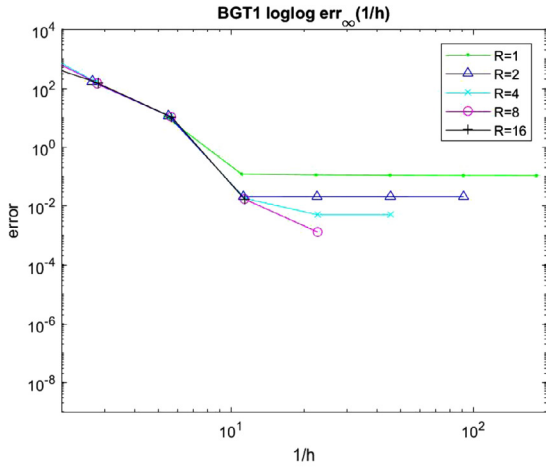
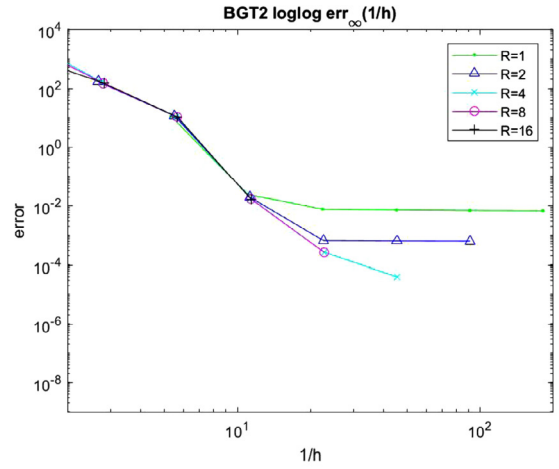


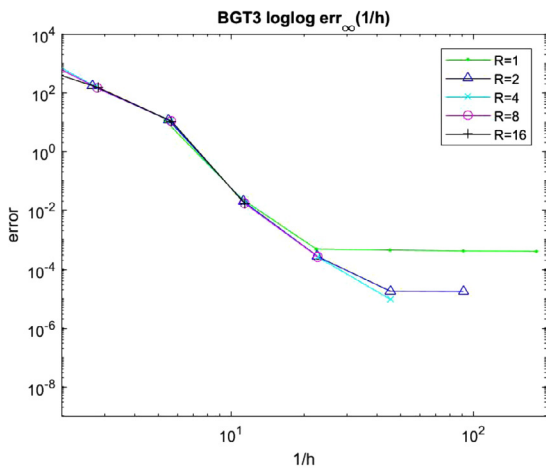
Fig. 1. Grid convergence for the case of a monopole: Maximum norm of the error as a function of the grid dimension for five specific values of R (radius of the spherical domain Ω). Individual graphs in each plot correspond to BGT ABCs of order 1 to 6; a reference graph is added in each plot for Dirichlet boundary conditions.



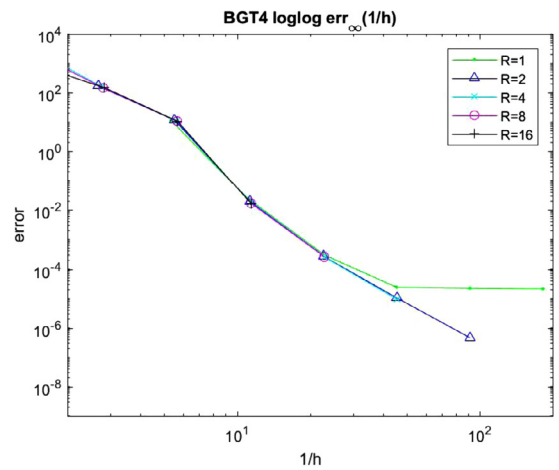
(a) BGT1



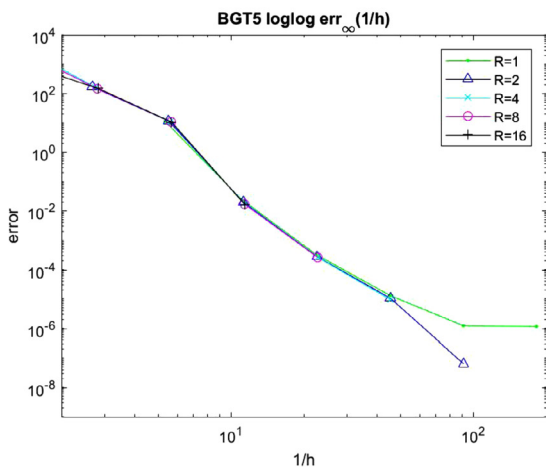
(b) BGT2



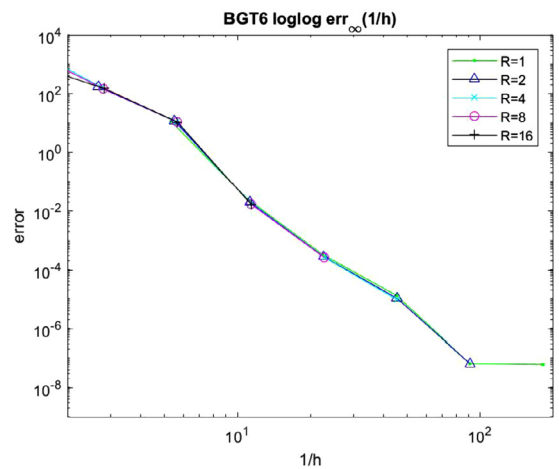
(c) BGT3



(d) BGT4



(e) BGT5



(f) BGT6

Fig. 2. Grid convergence for the case of a monopole: Maximum norm of the error as a function of the grid dimension for BGT ABCs of orders 1 through 6. Individual graphs in each plot correspond to spherical domains Ω of radius $R = 1, 2, 4, 8,$ and 16 .

Table 1
Overall error of numerical solution for the case of a monopole: Different grids, computational domains of radius $R = 1, 2, 4, 8,$ and $16,$ and BGT ABCs of order 1 through 3. The case of a Dirichlet boundary condition is included to provide a reference solution for comparison.

h	0.18666700		0.09032260		0.04444440		0.02204720		0.01098040		0.00547945	
R	error	rate										
1	1.114892e+01	N/A	2.366463e-02	8.9	3.234717e-04	6.2	1.298020e-05	4.6	6.396847e-08	7.7	9.787420e-10	6.0
2	1.220148e+01	3.9	1.954488e-02	9.3	2.750435e-04	6.2	1.049496e-05	4.7	6.349324e-08	7.4		
4	1.055505e+01	3.7	1.767913e-02	9.2	2.644951e-04	6.1	9.276481e-06	4.8				
8	1.114081e+01	3.7	1.649380e-02	9.4	2.599500e-04	6.0						
16	7.496487e+00	3.5	1.778119e-02	8.7								
(a) Dirichlet												
h	0.18666700		0.09032260		0.04444440		0.02204720		0.01098040		0.00547945	
R	error	rate										
1	1.136219e+01	N/A	1.206390e-01	6.6	1.136982e-01	0.1	1.105966e-01	0.0	1.083380e-01	0.0	1.072109e-01	0.0
2	1.165144e+01	3.9	2.050023e-02	9.2	2.064251e-02	0.0	2.058567e-02	0.0	2.054952e-02	0.0		
4	1.119331e+01	3.8	1.814784e-02	9.3	4.967169e-03	1.9	4.967923e-03	0.0				
8	1.086364e+01	3.8	1.697191e-02	9.3	1.278063e-03	3.7						
16	1.067608e+01	3.8	1.659104e-02	9.3								
(b) BGT1												
h	0.18666700		0.09032260		0.04444440		0.02204720		0.01098040		0.00547945	
R	error	rate										
1	1.136624e+01	N/A	2.438790e-02	8.9	7.667027e-03	1.7	7.239910e-03	0.1	6.936342e-03	0.1	6.787081e-03	0.0
2	1.165245e+01	3.9	1.983340e-02	9.2	6.508377e-04	4.9	6.321433e-04	0.0	6.227403e-04	0.0		
4	1.119315e+01	3.8	1.788809e-02	9.3	2.646931e-04	6.1	3.886825e-05	2.8				
8	1.086370e+01	3.8	1.699967e-02	9.3	2.595027e-04	6.0						
16	1.067606e+01	3.8	1.658079e-02	9.3								
(c) BGT2												
h	0.18666700		0.09032260		0.04444440		0.02204720		0.01098040		0.00547945	
R	error	rate										
1	1.136617e+01	N/A	2.438910e-02	8.9	4.699177e-04	5.7	4.307192e-04	0.1	4.037733e-04	0.1	3.907266e-04	0.0
2	1.165245e+01	3.9	1.983234e-02	9.2	2.751376e-04	6.2	1.780606e-05	3.9	1.733089e-05	0.0		
4	1.119315e+01	3.8	1.788813e-02	9.3	2.645012e-04	6.1	9.323097e-06	4.8				
8	1.086370e+01	3.8	1.699967e-02	9.3	2.595077e-04	6.0						
16	1.067606e+01	3.8	1.658079e-02	9.3								
(d) BGT3												

Table 2Overall error of numerical solution for the case of a monopole: Different grids, computational domains of radius $R = 1, 2, 4, 8,$ and $16,$ and BGT ABCs of order 4 through 6.

h	0.18666700		0.09032260		0.04444440		0.02204720		0.01098040		0.00547945	
R	error	rate										
1	1.136617e+01	N/A	2.438911e-02	8.9	3.233914e-04	6.2	2.435547e-05	3.7	2.242375e-05	0.1	2.146180e-05	0.1
2	1.165245e+01	3.9	1.983234e-02	9.2	2.751231e-04	6.2	1.046451e-05	4.7	4.596993e-07	4.5		
4	1.119315e+01	3.8	1.788813e-02	9.3	2.645013e-04	6.1	9.323021e-06	4.8				
8	1.086370e+01	3.8	1.699967e-02	9.3	2.595077e-04	6.0						
16	1.067606e+01	3.8	1.658079e-02	9.3								

(a) BGT4

h	0.18666700		0.09032260		0.04444440		0.02204720		0.01098040		0.00547945	
R	error	rate										
1	1.136617e+01	N/A	2.438911e-02	8.9	3.233955e-04	6.2	1.303322e-05	4.6	1.210687e-06	3.4	1.146177e-06	0.1
2	1.165245e+01	3.9	1.983234e-02	9.2	2.751231e-04	6.2	1.046448e-05	4.7	6.347373e-08	7.4		
4	1.119315e+01	3.8	1.788813e-02	9.3	2.645013e-04	6.1	9.323021e-06	4.8				
8	1.086370e+01	3.8	1.699967e-02	9.3	2.595077e-04	6.0						
16	1.067606e+01	3.8	1.658079e-02	9.3								

(b) BGT5

h	0.18666700		0.09032260		0.04444440		0.02204720		0.01098040		0.00547945	
R	error	rate										
1	1.136617e+01	N/A	2.438911e-02	8.9	3.233954e-04	6.2	1.303325e-05	4.6	6.419941e-08	7.7	6.007187e-08	0.1
2	1.165245e+01	3.9	1.983234e-02	9.2	2.751231e-04	6.2	1.046448e-05	4.7	6.347370e-08	7.4		
4	1.119315e+01	3.8	1.788813e-02	9.3	2.645013e-04	6.1	9.323021e-06	4.8				
8	1.086370e+01	3.8	1.699967e-02	9.3	2.595077e-04	6.0						
16	1.067606e+01	3.8	1.658079e-02	9.3								

(c) BGT6

purposes, in Table 1a we also include the values of the error and the convergence rate for the case of a Dirichlet boundary condition set at the outer boundary Γ . The rationale behind including this case is that for the exact Dirichlet data the only source of error in numerical solution is the discretization error on the grid, i.e., there is no reflection error. Consequently, one can compare the values of the error in Table 1a against those in Tables 1b through 2c and see where exactly the discretization error becomes smaller than the reflection error. The exact Dirichlet data are obtained directly from evaluating the test solution (52) on Γ . As far as solving the Dirichlet problem for the Helmholtz equation (19), it is even easier than solving the problem with the boundary condition (21). All it takes is to substitute the Dirichlet coefficients $c_{ls}^{(0)}$ that are known in this case into system (47) and solve by least squares for the unknown Neumann coefficients $c_{ls}^{(1)}$. Equations (48) are not needed.

The data in Table 3 also correspond to Figs. 1 and 2. The relation between Table 3 and Tables 1 and 2 is similar to that between Fig. 2 and Fig. 1. Namely, individual sub-tables in Tables 1 and 2 refer to BGT ABCs of different orders, whereas rows in each sub-table correspond to different values of R . Conversely, individual sub-tables in Table 3 refer to different values of R , while rows in each sub-table correspond to different orders of the BGT ABCs.

5.3.2. Variation of k for a fixed R

In Figs. 3 and 4, we show the grid convergence of our algorithm in the case of an off center monopole source (Section 5.2) for a fixed $R = 1$ and several different values of k . Note that according to [32], the specific value of R should not significantly affect the performance of the ABCs as it depends on k . Individual panels in Fig. 3, i.e., Figs. 3a through 3e, correspond to the wavenumbers $k = 1, 2, 4, 8, 16$, and 32 , whereas individual graphs in each panel correspond to the BGT ABCs of order 1 through 6. Note that, Fig. 3a is the same as Fig. 1a. In every Figure from 3a to 3e, one can observe the design sixth order rate of grid convergence for the scheme until it reaches the level of the reflection error (that does not depend on the grid) and stops. For a given k , the higher the order of the BGT ABC the later it occurs, which is in accordance with the theoretical expectations, see equation (5). Moreover, as the wavenumber k increases, only the ABCs of lower orders keep causing a slowdown of grid convergence, whereas the ABCs of higher orders maintain convergence over the entire range of grids. This is also in accordance with the theoretical expectations.

Fig. 4 represents the same grid convergence data as Fig. 3 does, but organized differently. Individual plots in Fig. 4, i.e., Figs. 4a through 4f, correspond to BGT ABCs of order 1 through 6, respectively, and individual graphs in each plot show the convergence of the discrete solution on the domain Ω of a fixed radius $R = 1$ for the wavenumbers $k = 1, 2, 4, 8, 16$, and 32 . As expected, for a given order of the BGT ABC the scheme converges until the reflection error becomes larger than the discretization error. This occurs sooner for lower value of k (longer waves) and later for higher values of k (shorter waves).

Fig. 5 is the same as Fig. 3 except that the error is evaluated using the l_2 norm as opposed to the maximum norm. The respective plots in Figs. 5 and 3 are basically indistinguishable.

The data shown in Figs. 3, 4, and 5 are not presented in tables for the reason of compactness. For the same reason, we do not include the l_2 convergence plots for any other simulations except those in Fig. 5; yet they look very much alike for all the cases we have studied.

5.4. Dipole

Numerical results for the case of a dipole, i.e., the source term $f_d = Lu_d$ in equation (19), where u_d is given by (53), are presented in Figs. 6 and 7, as well as Tables 4, 5, and 6. The corresponding computational data are organized exactly the same way as in Figs. 1a and 2 and Tables 1, 2, and 3, respectively. Namely, the individual plots in Fig. 6 show the grid convergence graphs for a sequence of ABCs $m = 1, \dots, 6$ and several different values of R , whereas the individual plots in Fig. 7 show the grid convergence graphs for a sequence of radii R and different orders of the BGT ABCs. Tables 4 and 5 present the actual numerical values of the error and convergence rate arranged similarly to Fig. 6, whereas Table 6 does the same but in the order similar to that of Fig. 7.

The resulting observations are also similar to those we made in the case of a monopole, see Section 5.3. Specifically, the scheme demonstrates the design sixth order grid convergence all the way down until the discretization error becomes smaller than the reflection error and then the convergence ceases. The larger the radius R for a fixed order of the ABC, the later this occurs. The same is true for the ABCs of an increasing order and a fixed R .

We do not include here the results for a fixed R and varying k in the case of a dipole. These results are very similar to those presented in Section 5.3.2 for the case of a monopole.

6. Discussion

We have developed two separate ideas. The first one, given by (12), provides an explicit formula for the BGT operators using a recursion formula for their coefficients. In fact, we derive the completely explicit formulae through BGT order 6, see (4) and (13). We then show that if the solution is expanded in spherical harmonics according to (17) (eigenfunctions of the Beltrami operator), then the coefficients for the BGT expansion satisfy (18) and neither high order differences nor any auxiliary variables appear in BGT.

Table 3
 Overall error of numerical solution for the case of a monopole: Different grids, BGT ABCs of order 1 through 6, and computational domains of radius $R = 1, 2, 4, 8,$ and 16 . Dirichlet boundary condition is included for reference purposes.

R		error	rate	error	rate															
1	h							0.18666700		0.09032260		0.04444440		0.02204720		0.01098040		0.00547945		
	Dir							1.114892e+01	N/A	2.366463e-02	8.9	3.234717e-04	6.2	1.298020e-05	4.6	6.396847e-08	7.7	9.787420e-10	6.0	
	BGT1							1.136219e+01	N/A	1.206390e-01	6.6	1.136982e-01	0.1	1.105966e-01	0.0	1.083380e-01	0.0	1.072109e-01	0.0	0.0
	BGT2							1.136624e+01	N/A	2.438790e-02	8.9	7.667027e-03	1.7	7.239910e-03	0.1	6.936342e-03	0.1	6.787081e-03	0.0	0.0
	BGT3							1.136617e+01	N/A	2.438910e-02	8.9	4.699177e-04	5.7	4.307192e-04	0.1	4.037733e-04	0.1	3.907266e-04	0.0	0.0
	BGT4							1.136617e+01	N/A	2.438911e-02	8.9	3.233914e-04	6.2	2.435547e-05	3.7	2.242375e-05	0.1	2.146180e-05	0.1	0.1
	BGT5							1.136617e+01	N/A	2.438911e-02	8.9	3.233955e-04	6.2	1.303322e-05	4.6	1.210687e-06	3.4	1.146177e-06	0.1	0.1
BGT6							1.136617e+01	N/A	2.438911e-02	8.9	3.233954e-04	6.2	1.303325e-05	4.6	6.419941e-08	7.7	6.007187e-08	0.1	0.1	
2	h					0.37333300		0.18064500		0.08888890		0.04409450		0.02196080		0.01095890				
	Dir							1.826566e+02	N/A	1.220148e+01	3.9	1.954488e-02	9.3	2.750435e-04	6.2	1.049496e-05	4.7	6.349324e-08	7.4	
	BGT1							1.705997e+02	N/A	1.165144e+01	3.9	2.050023e-02	9.2	2.064251e-02	-0.0	2.058567e-02	0.0	2.054952e-02	0.0	0.0
	BGT2							1.707045e+02	N/A	1.165245e+01	3.9	1.983340e-02	9.2	6.508377e-04	4.9	6.321433e-04	0.0	6.227403e-04	0.0	0.0
	BGT3							1.707046e+02	N/A	1.165245e+01	3.9	1.983234e-02	9.2	2.751376e-04	6.2	1.780606e-05	3.9	1.733089e-05	0.0	0.0
	BGT4							1.707046e+02	N/A	1.165245e+01	3.9	1.983234e-02	9.2	2.751231e-04	6.2	1.046451e-05	4.7	4.596993e-07	4.5	
	BGT5							1.707046e+02	N/A	1.165245e+01	3.9	1.983234e-02	9.2	2.751231e-04	6.2	1.046448e-05	4.7	6.347373e-08	7.4	
BGT6							1.707046e+02	N/A	1.165245e+01	3.9	1.983234e-02	9.2	2.751231e-04	6.2	1.046448e-05	4.7	6.347370e-08	7.4		
4	h			0.74666700		0.36129000		0.17777800		0.08818900		0.04392160		0.02191780						
	Dir							3.737077e+03	N/A	1.380857e+02	4.8	1.055505e+01	3.7	1.767913e-02	9.2	2.644951e-04	6.1	9.276481e-06	4.8	
	BGT1							4.230011e+03	N/A	1.603206e+02	4.7	1.119331e+01	3.8	1.814784e-02	9.3	4.967169e-03	1.9	4.967923e-03	-0.0	
	BGT2							4.223648e+03	N/A	1.602978e+02	4.7	1.119315e+01	3.8	1.788809e-02	9.3	2.646931e-04	6.1	3.886825e-05	2.8	
	BGT3							4.223683e+03	N/A	1.602978e+02	4.7	1.119315e+01	3.8	2.645012e-04	6.1	9.323097e-06	4.8			
	BGT4							4.223683e+03	N/A	1.602978e+02	4.7	1.119315e+01	3.8	1.788813e-02	9.3	2.645013e-04	6.1	9.323021e-06	4.8	
	BGT5							4.223683e+03	N/A	1.602978e+02	4.7	1.119315e+01	3.8	1.788813e-02	9.3	2.645013e-04	6.1	9.323021e-06	4.8	
BGT6							4.223683e+03	N/A	1.602978e+02	4.7	1.119315e+01	3.8	1.788813e-02	9.3	2.645013e-04	6.1	9.323021e-06	4.8		
8	h		1.49333000		0.72258100		0.35556000		0.17637800		0.08784310		0.04383560							
	Dir							7.570284e-01	N/A	2.575025e+03	-11.7	1.470459e+02	4.1	1.114081e+01	3.7	1.649380e-02	9.4	2.599500e-04	6.0	
	BGT1							8.928097e-01	N/A	2.783931e+03	-11.6	1.468097e+02	4.2	1.086364e+01	3.8	1.697191e-02	9.3	1.278063e-03	3.7	
	BGT2							8.928097e-01	N/A	2.784109e+03	-11.6	1.468114e+02	4.2	1.086370e+01	3.8	1.699967e-02	9.3	2.595077e-04	6.0	
	BGT3							8.928097e-01	N/A	2.784109e+03	-11.6	1.468114e+02	4.2	1.086370e+01	3.8	1.699967e-02	9.3	2.595077e-04	6.0	
	BGT4							8.928097e-01	N/A	2.784109e+03	-11.6	1.468114e+02	4.2	1.086370e+01	3.8	1.699967e-02	9.3	2.595077e-04	6.0	
	BGT5							8.928097e-01	N/A	2.784109e+03	-11.6	1.468114e+02	4.2	1.086370e+01	3.8	1.699967e-02	9.3	2.595077e-04	6.0	
BGT6							8.928097e-01	N/A	2.784109e+03	-11.6	1.468114e+02	4.2	1.086370e+01	3.8	1.699967e-02	9.3	2.595077e-04	6.0		
16	h	2.98667000		1.44516000		0.71111100		0.35275600		0.17568600		0.08767120								
	Dir	2.465302e+00	N/A	2.510902e+00	-0.0	4.973982e+02	-7.6	7.496487e+00	2.5	1.778119e+02	3.5	1.778119e+02	8.7							
	BGT1	4.143662e-01	N/A	9.273502e-01	-1.2	9.950493e+02	-10.1	1.502829e+02	2.7	1.067608e+01	3.8	1.659104e-02	9.3							
	BGT2	4.143662e-01	N/A	9.273502e-01	-1.2	9.950161e+02	-10.1	1.502820e+02	2.7	1.067606e+01	3.8	1.658079e-02	9.3							
	BGT3	4.143662e-01	N/A	9.273502e-01	-1.2	9.950161e+02	-10.1	1.502820e+02	2.7	1.067606e+01	3.8	1.658079e-02	9.3							
	BGT4	4.143662e-01	N/A	9.273502e-01	-1.2	9.950161e+02	-10.1	1.502820e+02	2.7	1.067606e+01	3.8	1.658079e-02	9.3							
	BGT5	4.143662e-01	N/A	9.273502e-01	-1.2	9.950161e+02	-10.1	1.502820e+02	2.7	1.067606e+01	3.8	1.658079e-02	9.3							
BGT6	4.143662e-01	N/A	9.273502e-01	-1.2	9.950161e+02	-10.1	1.502820e+02	2.7	1.067606e+01	3.8	1.658079e-02	9.3								

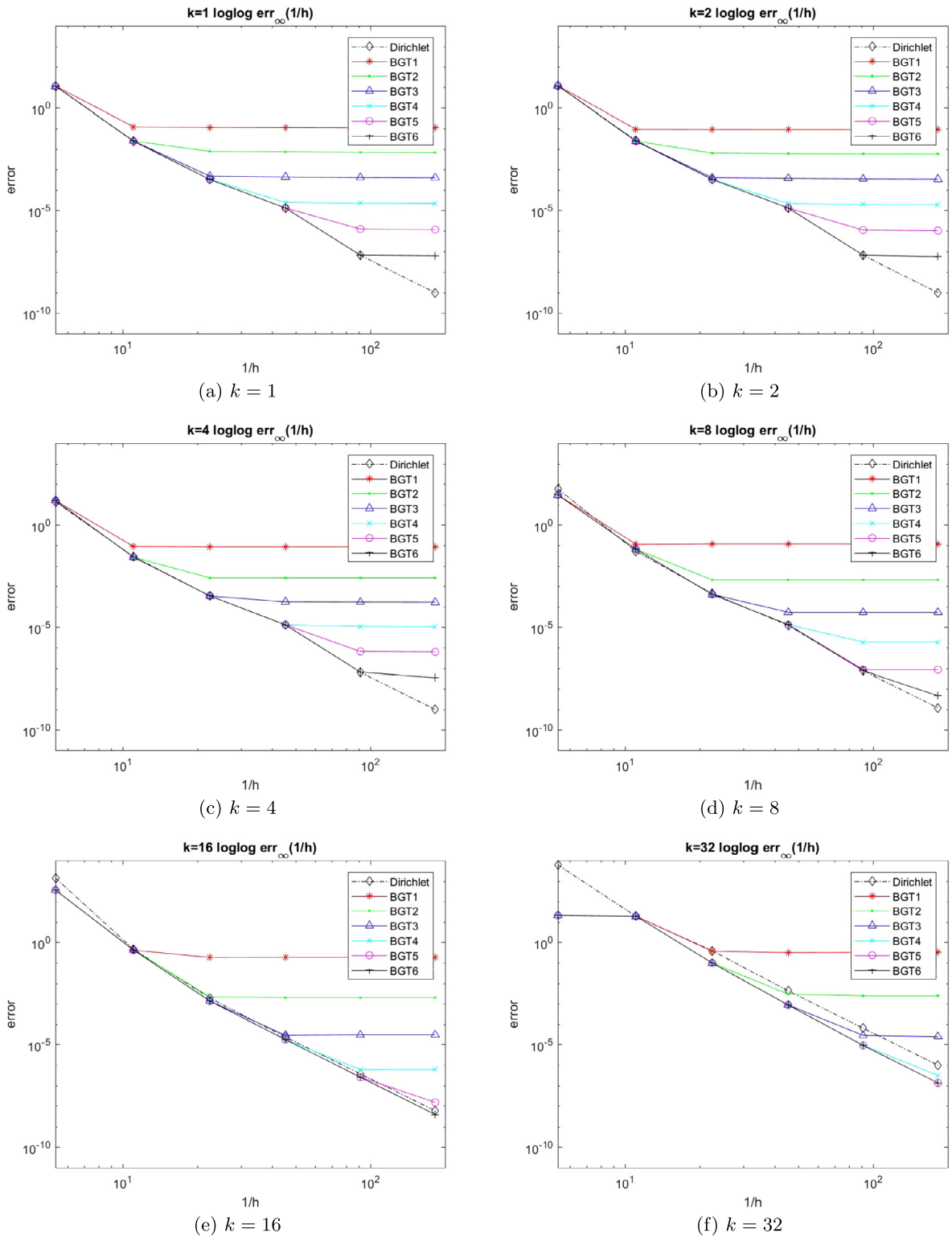


Fig. 3. Grid convergence for the case of a monopole: Maximum norm of the error as a function of the grid dimension on a fixed domain Ω of radius $R = 1$ for six different values of the wavenumber k . Individual graphs in each plot correspond to BGT ABCs of order 1 to 6; a reference graph is added in each plot for Dirichlet boundary conditions.

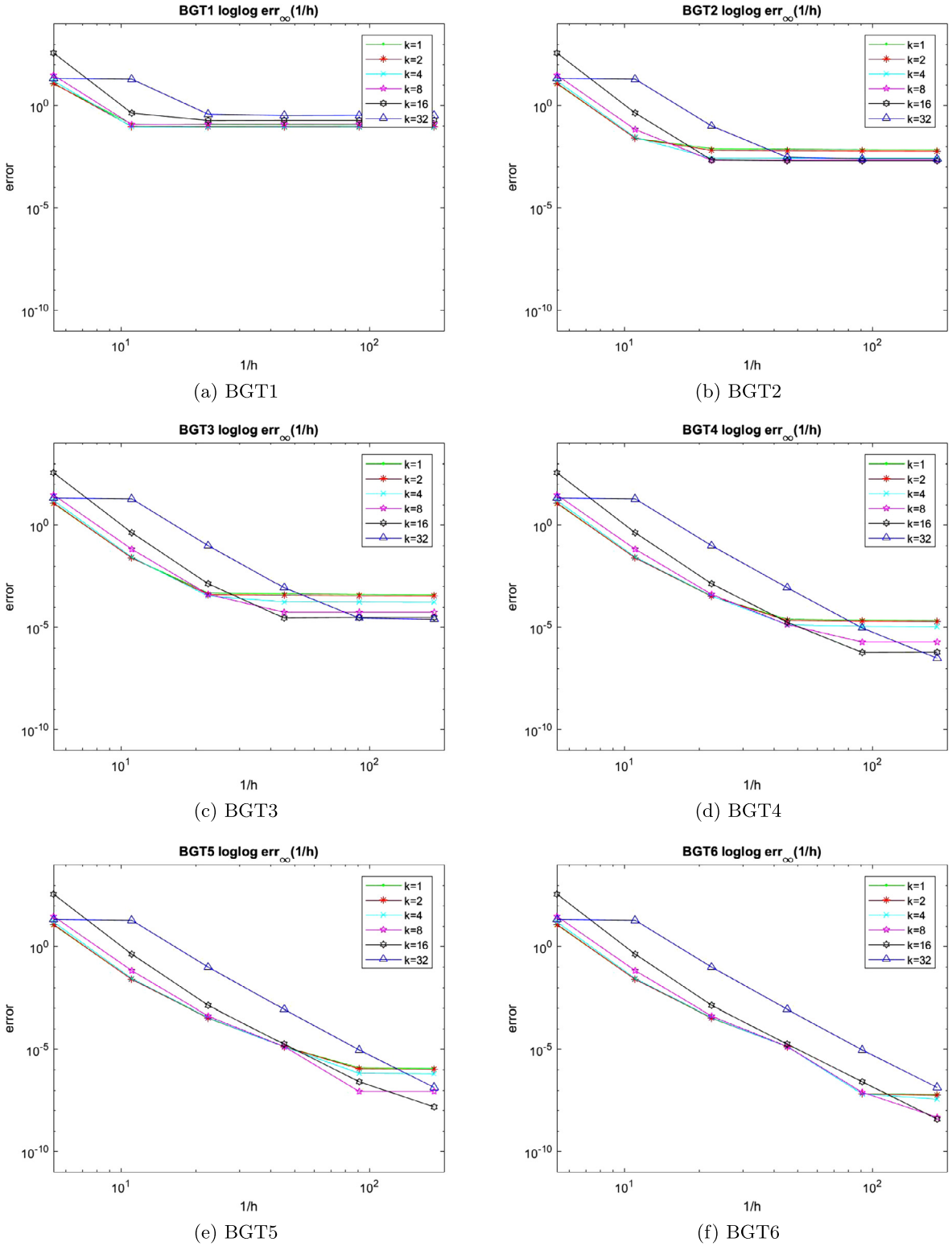


Fig. 4. Grid convergence for the case of a monopole: Maximum norm of the error as a function of the grid dimension on the domain Ω of a fixed radius $R = 1$ for BGT ABCs of orders 1 through 6. Individual graphs in each plot correspond to the wavenumbers $k = 1, 2, 4, 8, 16,$ and 32 .

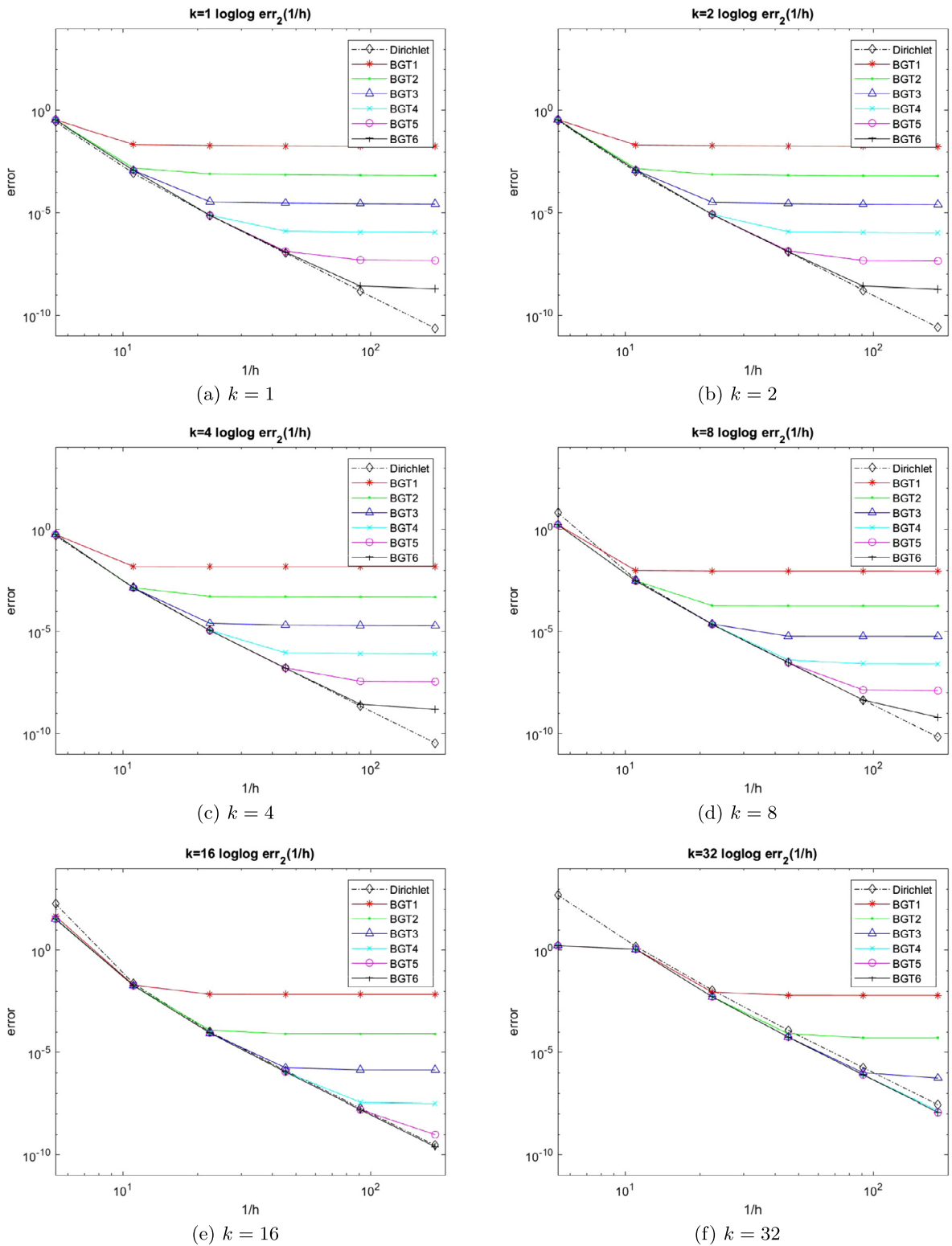


Fig. 5. Grid convergence for the case of a monopole: l_2 norm of the error as a function of the grid dimension on the domain Ω of a fixed radius $R = 1$ for six different values of the wavenumber k . Individual graphs in each plot correspond to BGT ABCs of order 1 to 6; a reference graph is added in each plot for Dirichlet boundary conditions.

Table 4
Overall error of numerical solution for the case of a dipole: Different grids, computational domains of radius $R = 1, 2, 4, 8,$ and $16,$ and BGT ABCs of order 1 through 3. The case of a Dirichlet boundary condition is included to provide a reference solution for comparison.

h	0.18666700		0.09032260		0.04444440		0.02204720		0.01098040		0.00547945	
R	error	rate										
1	2.176768e+01	N/A	1.102305e-01	7.6	1.509871e-03	6.2	1.829264e-05	6.4	2.818531e-07	6.0	6.121860e-09	5.5
2	1.953732e+01	5.7	1.014012e-01	7.6	1.456399e-03	6.1	1.792210e-05	6.3	2.788377e-07	6.0		
4	1.714217e+01	5.2	9.634636e-02	7.5	1.422687e-03	6.1	1.770789e-05	6.3				
8	1.704826e+01	5.0	9.586761e-02	7.5	1.410661e-03	6.1						
16	1.508012e+01	5.4	9.005339e-02	7.4								
(a) Dirichlet												
h	0.18666700		0.09032260		0.04444440		0.02204720		0.01098040		0.00547945	
R	error	rate										
1	2.226624e+01	N/A	7.797153e-01	4.8	7.441768e-01	0.1	7.136860e-01	0.1	7.022265e-01	0.0	6.951053e-01	0.0
2	1.921565e+01	5.6	1.229326e-01	7.3	1.233793e-01	-0.0	1.230037e-01	0.0	1.228049e-01	0.0		
4	1.768602e+01	5.1	9.653701e-02	7.5	2.903638e-02	1.7	2.903905e-02	-0.0				
8	1.696009e+01	5.1	9.578361e-02	7.5	7.549767e-03	3.7						
16	1.660575e+01	5.0	9.482681e-02	7.5								
(b) BGT1												
h	0.18666700		0.09032260		0.04444440		0.02204720		0.01098040		0.00547945	
R	error	rate										
1	2.227855e+01	N/A	1.106727e-01	7.7	9.132616e-02	0.3	8.442000e-02	0.1	8.111395e-02	0.1	7.938693e-02	0.0
2	1.920440e+01	5.6	1.009493e-01	7.6	7.006303e-03	3.8	6.853073e-03	0.0	6.763905e-03	0.0		
4	1.768844e+01	5.1	9.739239e-02	7.5	1.421401e-03	6.1	4.049162e-04	1.8				
8	1.695986e+01	5.1	9.569406e-02	7.5	1.410478e-03	6.1						
16	1.660583e+01	5.0	9.485976e-02	7.5								
(c) BGT2												
h	0.18666700		0.09032260		0.04444440		0.02204720		0.01098040		0.00547945	
R	error	rate										
1	2.227864e+01	N/A	1.106897e-01	7.7	7.916120e-03	3.8	7.138485e-03	0.1	6.785685e-03	0.1	6.590410e-03	0.0
2	1.920445e+01	5.6	1.009539e-01	7.6	1.454561e-03	6.1	2.796994e-04	2.4	2.729840e-04	0.0		
4	1.768844e+01	5.1	9.739222e-02	7.5	1.425456e-03	6.1	1.772142e-05	6.3				
8	1.695986e+01	5.1	9.569406e-02	7.5	1.410325e-03	6.1						
16	1.660583e+01	5.0	9.485976e-02	7.5								
(d) BGT3												

Table 5Overall error of numerical solution for the case of a dipole: Different grids, computational domains of radius $R = 1, 2, 4, 8,$ and $16,$ and BGT ABCs of order 4 through 6.

h	0.18666700		0.09032260		0.04444440		0.02204720		0.01098040		0.00547945		
	R	error	rate	error	rate	error	rate	error	rate	error	rate	error	rate
1	2.227864e+01	N/A		1.106895e-01	7.7	1.511627e-03	6.2	5.317557e-04	1.5	4.884095e-04	0.1	4.713655e-04	0.1
2	1.920445e+01	5.6		1.009539e-01	7.6	1.455074e-03	6.1	1.791555e-05	6.3	9.496799e-06	0.9		
4	1.768844e+01	5.1		9.739222e-02	7.5	1.425452e-03	6.1	1.772115e-05	6.3				
8	1.695986e+01	5.1		9.569406e-02	7.5	1.410325e-03	6.1						
16	1.660583e+01	5.0		9.485976e-02	7.5								

(a) BGT4

h	0.18666700		0.09032260		0.04444440		0.02204720		0.01098040		0.00547945		
	R	error	rate	error	rate	error	rate	error	rate	error	rate	error	rate
1	2.227864e+01	N/A		1.106895e-01	7.7	1.511402e-03	6.2	3.613601e-05	5.4	3.260396e-05	0.1	3.116217e-05	0.1
2	1.920445e+01	5.6		1.009539e-01	7.6	1.455072e-03	6.1	1.791544e-05	6.3	3.018865e-07	5.9		
4	1.768844e+01	5.1		9.739222e-02	7.5	1.425452e-03	6.1	1.772115e-05	6.3				
8	1.695986e+01	5.1		9.569406e-02	7.5	1.410325e-03	6.1						
16	1.660583e+01	5.0		9.485976e-02	7.5								

(b) BGT5

h	0.18666700		0.09032260		0.04444440		0.02204720		0.01098040		0.00547945		
	R	error	rate	error	rate	error	rate	error	rate	error	rate	error	rate
1	2.227864e+01	N/A		1.106895e-01	7.7	1.511406e-03	6.2	1.830059e-05	6.4	2.050694e-06	3.2	1.951438e-06	0.1
2	1.920445e+01	5.6		1.009539e-01	7.6	1.455072e-03	6.1	1.791544e-05	6.3	2.788349e-07	6.0		
4	1.768844e+01	5.1		9.739222e-02	7.5	1.425452e-03	6.1	1.772115e-05	6.3				
8	1.695986e+01	5.1		9.569406e-02	7.5	1.410325e-03	6.1						
16	1.660583e+01	5.0		9.485976e-02	7.5								

(c) BGT6

Table 6
 Overall error of numerical solution for the case of a dipole: Different grids, BGT ABCs of order 1 through 6, and computational domains of radius $R = 1, 2, 4, 8,$ and 16 . Dirichlet boundary condition is included for reference purposes.

R		error	rate	error	rate	error	rate																
1	h							0.18666700		0.09032260		0.04444440		0.02204720		0.01098040		0.00547945					
	Dir							2.17678e+01	N/A	1.102305e-01	7.6	1.509871e-03	6.2	1.829264e-05	6.4	2.818531e-07	6.0	6.121860e-09	5.5				
	BGT1							2.226624e+01	N/A	7.797153e-01	4.8	7.441768e-01	0.1	7.136860e-01	0.1	7.022265e-01	0.0	6.951053e-01	0.0				
	BGT2							2.227855e+01	N/A	1.106727e-01	7.7	9.132616e-02	0.3	8.442000e-02	0.1	8.111395e-02	0.1	7.938693e-02	0.0				
	BGT3							2.227864e+01	N/A	1.106897e-01	7.7	7.916120e-03	3.8	7.138485e-03	0.1	6.785685e-03	0.1	6.590410e-03	0.0				
	BGT4							2.227864e+01	N/A	1.106895e-01	7.7	1.511627e-03	6.2	5.317557e-04	1.5	4.884095e-04	0.1	4.713655e-04	0.1				
	BGT5							2.227864e+01	N/A	1.106895e-01	7.7	1.511402e-03	6.2	3.613601e-05	5.4	3.260396e-05	0.1	3.116217e-05	0.1				
BGT6							2.227864e+01	N/A	1.106895e-01	7.7	1.511406e-03	6.2	1.830059e-05	6.4	2.050694e-06	3.2	1.951438e-06	0.1					
2	h			0.37333300		0.18064500		0.08888890		0.04409450		0.02196080		0.01095890									
	Dir			9.943408e+02	N/A	1.953732e+01	5.7	1.014012e-01	7.6	1.456399e-03	6.1	1.792210e-05	6.3	2.788377e-07	6.0								
	BGT1			9.561972e+02	N/A	1.921565e+01	5.6	1.229326e-01	7.3	1.233793e-01	-0.0	1.230037e-01	0.0	1.228049e-01	0.0								
	BGT2			9.568898e+02	N/A	1.920440e+01	5.6	1.009493e-01	7.6	7.006303e-03	3.8	6.853073e-03	0.0	6.763905e-03	0.0								
	BGT3			9.568844e+02	N/A	1.920445e+01	5.6	1.009539e-01	7.6	1.454561e-03	6.1	2.796994e-04	2.4	2.729840e-04	0.0								
	BGT4			9.568844e+02	N/A	1.920445e+01	5.6	1.009539e-01	7.6	1.455074e-03	6.1	1.791555e-05	6.3	9.496799e-06	0.9								
	BGT5			9.568844e+02	N/A	1.920445e+01	5.6	1.009539e-01	7.6	1.455072e-03	6.1	1.791544e-05	6.3	3.01885e-07	5.9								
BGT6			9.568844e+02	N/A	1.920445e+01	5.6	1.009539e-01	7.6	1.455072e-03	6.1	1.791544e-05	6.3	2.788349e-07	6.0									
4	h			0.74666700		0.36129000		0.17777800		0.08818900		0.04392160		0.02191780									
	Dir			1.804114e+03	N/A	6.153403e+02	1.6	1.714217e+01	5.2	9.634636e-02	7.5	1.422687e-03	6.1	1.770789e-05	6.3								
	BGT1			2.043237e+03	N/A	6.258716e+02	1.7	1.768602e+01	5.1	9.653701e-02	7.5	2.903638e-02	1.7	2.903905e-02	-0.0								
	BGT2			2.040161e+03	N/A	6.257024e+02	1.7	1.768844e+01	5.1	9.739239e-02	7.5	1.421401e-03	6.1	4.049162e-04	1.8								
	BGT3			2.040178e+03	N/A	6.257026e+02	1.7	1.768844e+01	5.1	9.739222e-02	7.5	1.425456e-03	6.1	1.772142e-05	6.3								
	BGT4			2.040177e+03	N/A	6.257026e+02	1.7	1.768844e+01	5.1	9.739222e-02	7.5	1.425452e-03	6.1	1.772115e-05	6.3								
	BGT5			2.040177e+03	N/A	6.257026e+02	1.7	1.768844e+01	5.1	9.739222e-02	7.5	1.425452e-03	6.1	1.772115e-05	6.3								
BGT6			2.040177e+03	N/A	6.257026e+02	1.7	1.768844e+01	5.1	9.739222e-02	7.5	1.425452e-03	6.1	1.772115e-05	6.3									
8	h		1.49333000		0.72258100		0.35555600		0.17637800		0.08784310		0.04383560										
	Dir		4.894104e+00	N/A	6.771435e+03	-10.4	5.625001e+02	3.6	1.704826e+01	5.0	9.586761e-02	7.5	1.410661e-03	6.1									
	BGT1		6.988980e-01	N/A	7.320852e+03	-13.4	5.744309e+02	3.7	1.696009e+01	5.1	9.578361e-02	7.5	7.549767e-03	3.7									
	BGT2		6.988980e-01	N/A	7.321320e+03	-13.4	5.744464e+02	3.7	1.695986e+01	5.1	9.569406e-02	7.5	1.410478e-03	6.1									
	BGT3		6.988980e-01	N/A	7.321319e+03	-13.4	5.744464e+02	3.7	1.695986e+01	5.1	9.569406e-02	7.5	1.410325e-03	6.1									
	BGT4		6.988980e-01	N/A	7.321319e+03	-13.4	5.744464e+02	3.7	1.695986e+01	5.1	9.569406e-02	7.5	1.410325e-03	6.1									
	BGT5		6.988980e-01	N/A	7.321319e+03	-13.4	5.744464e+02	3.7	1.695986e+01	5.1	9.569406e-02	7.5	1.410325e-03	6.1									
BGT6		6.988980e-01	N/A	7.321319e+03	-13.4	5.744464e+02	3.7	1.695986e+01	5.1	9.569406e-02	7.5	1.410325e-03	6.1										
16	h	2.98667000		1.44516000		0.71111100		0.35275600		0.17568600		0.08767120											
	Dir	1.763344e+01	N/A	8.560909e-01	4.4	4.388879e+03	-12.3	6.368976e+02	2.8	1.508012e+01	5.4	9.380359e-02	7.4										
	BGT1	2.667474e-01	N/A	7.362783e-01	-1.5	8.748258e+03	-13.5	5.475294e+02	4.0	1.660575e+01	5.0	9.482681e-02	7.5										
	BGT2	2.667474e-01	N/A	7.362783e-01	-1.5	8.747967e+03	-13.5	5.475240e+02	4.0	1.660583e+01	5.0	9.485976e-02	7.5										
	BGT3	2.667474e-01	N/A	7.362783e-01	-1.5	8.747967e+03	-13.5	5.475240e+02	4.0	1.660583e+01	5.0	9.485976e-02	7.5										
	BGT4	2.667474e-01	N/A	7.362783e-01	-1.5	8.747967e+03	-13.5	5.475240e+02	4.0	1.660583e+01	5.0	9.485976e-02	7.5										
	BGT5	2.667474e-01	N/A	7.362783e-01	-1.5	8.747967e+03	-13.5	5.475240e+02	4.0	1.660583e+01	5.0	9.485976e-02	7.5										
BGT6	2.667474e-01	N/A	7.362783e-01	-1.5	8.747967e+03	-13.5	5.475240e+02	4.0	1.660583e+01	5.0	9.485976e-02	7.5											

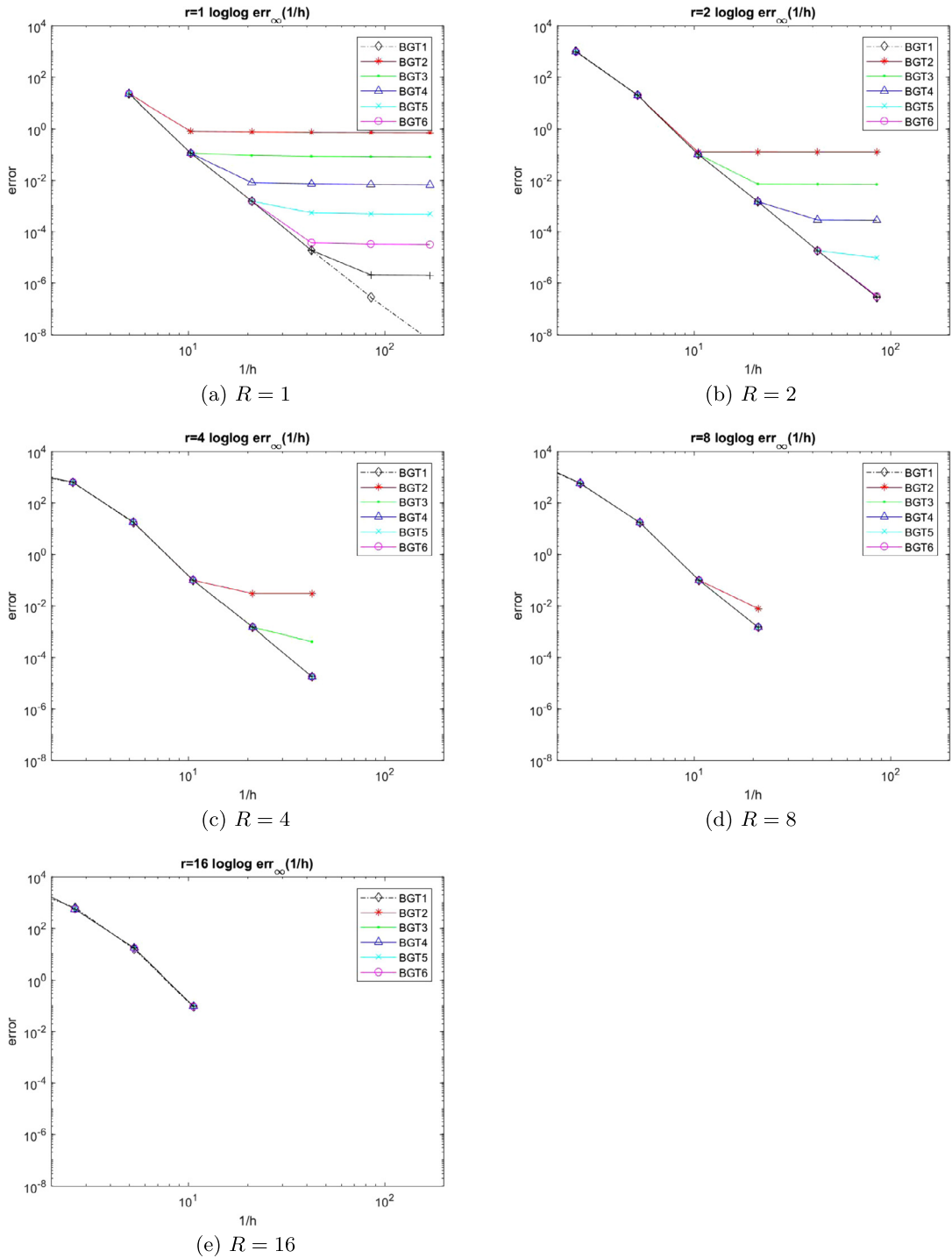


Fig. 6. Grid convergence for the case of a dipole: Maximum norm of the error as a function of the grid dimension for five specific values of R (radius of the spherical domain Ω). Individual graphs in each plot correspond to BGT ABCs of order 1 to 6.

In order to efficiently implement the high order BGT, we couple it with a compact high order finite difference scheme using difference potentials. Future research will study ways of coupling (18) with a finite difference or finite element scheme without using difference potentials.

Results are presented for the Helmholtz equation with monopole and dipole sources displaced from the origin of the Cartesian grid. Computations confirm the sixth order accuracy of the combined high order difference scheme with the high

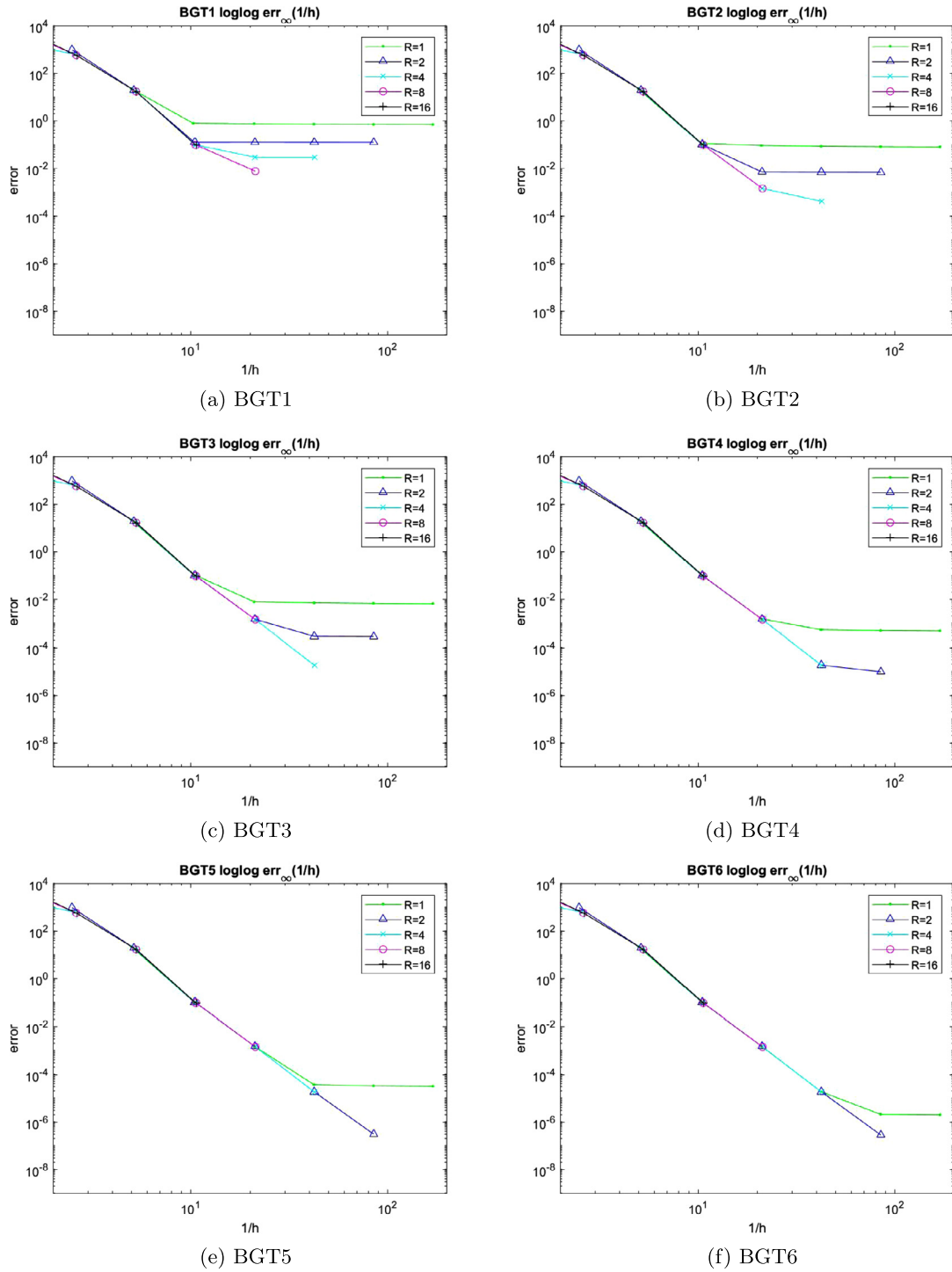


Fig. 7. Grid convergence for the case of a dipole: Maximum norm of the error as a function of the grid dimension for BGT ABCs of orders 1 through 6. Individual graphs in each plot correspond to spherical domains Ω of radius $R = 1, 2, 4, 8,$ and 16 .

order BGT artificial boundary condition. As expected, if the artificial outer boundary is far away, then the higher order BGT doesn't improve the accuracy. As the outer boundary is brought in closer, higher order BGT is needed to preserve the high accuracy of the interior scheme. This behavior corroborates the theoretical properties of the BGT ABCs that are built in by their design. A similar behavior that meets the theoretical expectations has been observed in the case of a fixed R and varying wavenumber k .

